Open Access

Recent Progress in Materials

LIDSEN Publishing Inc.

Review

Recent Developments in Synthesis Techniques and Microwave Absorption Performance of Materials Based on Molybdenum Disulfide (MoS_2) with Metal Oxides: A Review

Yusuf Sani [1, 2], Raba'ah Syahidah Azis [1, 3, *], Ismayadi Ismail [1], Yazid Yaakob [3], Chen Soo Kien [1, 3], Mohd Mustafa Awang Kechik [3], Lim Kean Pah [3]

1. Materials Synthesis and Characterization Laboratory (MSCL), Institute of Nanoscience and Nanotechnology (IONS), University Putra Malaysia, 43400 UPM Serdang, Selangor, Malaysia; E-Mails: yusufsani480@gmail.com; rabaah@upm.edu.my; ismayadi@upm.edu.my; chensk@upm.edu.my
2. Department of Pure and Applied Physics, Federal University Wukari, P.M.B 1020, Taraba State Nigeria
3. Department of Physics, Faculty of Science, University Putra Malaysia, 43400 UPM Serdang, Selangor Darul Ehsan, Malaysia; E-Mails: yazidakob@upm.edu.my; mmak@upm.edu.my; limkp@upm.edu.my

* **Correspondence:** Raba'ah Syahidah Azis; E-Mail: rabaah@upm.edu.my

Academic Editor: Changming Fang

Recent Progress in Materials
2025, volume 7, issue 1
doi:10.21926/rpm.2501003

Received: October 11, 2024
Accepted: December 25, 2024
Published: January 26, 2025

Abstract

The widespread usage of various wireless equipment in many facets of life has significantly contributed to the severe pollution caused by electromagnetic radiation. Thankfully, scientists have created materials that can absorb microwave radiation and convert dangerous electromagnetic waves into other forms of energy, including heat energy. Many recent investigations have been published regarding developing materials that absorb microwaves with different constituents, morphologies, and architectures. Microwave-absorbing materials (MAMs) are becoming more and more popular for use in a variety of aviation applications, including EMI prevention, information security, and reducing the risks of electromagnetic radiation to human health. Molybdenum di-sulphide (MoS_2) is a transition metal sulphide

extensively employed as a microwave absorption material (MAM) owing to its superior structural and physicochemical qualities. Because of its many flaws, huge specific surface area, and semiconductor qualities, MoS_2 exhibits exceptional microwave loss properties. Using several designs, MoS_2 may efficiently boost the absorption and dispersion of microwaves inside the absorber. This study introduces the structure, characteristics, and synthesis method based on MoS_2 material. This study provides an in-depth analysis of MoS_2-based microwave absorption materials (MAMs) and their improved absorption capabilities when combined with metal oxides. The results highlight that MoS_2-metal oxide composites exhibit enhanced microwave absorption efficiency, with detailed insights into the mechanisms driving this performance for various applications. Furthermore, the key problems and development challenges are examined, and the most recent advancements in MoS_2-based MAMs are impartially assessed and discussed. As a result, it is anticipated that MoS_2-based composites would provide excellent choices for very thin and light MAMs.

Keywords
Molybdenum sulphide; microwave; absorbing material; electromagnetic; radiation

1. Introduction

The widespread use of electronics and the swift advancement of wireless technologies are experiencing rapid expansion. This exacerbates electromagnetic pollution, which is the primary contributor to physical pollution and poses a substantial threat to public health [1, 2]. Creating advanced microwave absorption materials is the greatest solution to this issue. These substances can convert electromagnetic energy into thermal energy without producing any additional pollutants [3]. When examining potential uses, the perfect microwave absorber should possess a broad absorption bandwidth, minimal weight, thin thickness, and corrosion resistance [4, 5]. In contrast to traditional electromagnetic shielding materials, microwave absorbers are considered a more efficient approach for managing electromagnetic pollution [6]. When it comes to reducing electromagnetic interference, magnetic and dielectric losses make up the primary mechanisms in microwave absorbers [7]. Typical single-loss (dielectric or magnetic) microwave absorption materials often struggle to satisfy the demands of practical uses [8]. Therefore, there is a growing interest in microwave absorption regarding the utilization of materials that incorporate multiple loss mechanisms, whether magnetic or dielectric, to address this concern. The electromagnetic component of magnetic/dielectric composites may be artificially modified to increase microwave absorption [9] ammeters and impedance matching [10, 11]. As per the fundamental equation, when both the permeability $\mu_r = \mu' + j\mu''$ and the dielectric constant $\varepsilon_r = \varepsilon' + j\varepsilon''$ are identical, the incident wave can penetrate the material entirely without any reflection. Additionally, the attenuation characteristics are influenced by the loss mechanism, which comprises magnetic loss, dielectric loss, and conductivity loss.

Nanocomposites made of different ferrites and molybdenum disulfide (MoS_2) have been thoroughly studied to solve these problems. High-quality absorbers may be made from two-dimensional materials with extremely thin layers because they have outstanding electrical

characteristics and a large specific surface area [12]. Transition metal sulphide is thought to be the greatest material for electromagnetic wave absorption because of its very tiny band gaps, unusual shapes, and remarkable dielectric properties.

In recent years, scientists have learned that MoS_2 has excellent dielectric loss properties and is lightweight, making it a preferred material for the construction of portable electromagnetic absorbers. However, the material's high permeability and low permittivity make it hard to meet the standards for new wave-absorbing materials [13]. Recent studies have shown that some ferromagnetic and MoS_2 material blends perform very well in terms of microwave absorption. A hydrothermal process may be used to create high-purity MoS_2 [14]. MoS_2 is a significant component of 2D materials that has excellent interfacial polarisation and dielectric loss characteristics because of its high specific surface area and semiconductor characteristics. The single-atom thickness and multiple atomic layers of MoS_2's surface offer the design framework and support for microwave absorption materials (MAMs) [15]. Additionally, van der Waal forces, which promote numerous microwave reflections, cause the layered MoS_2 to stack. The microwaves may penetrate and attenuate due to the small layer thickness. Furthermore, various controlled structures with broadband absorption may be designed using 2D materials as structural elements. Additionally, research has shown that eddy currents may be successfully mitigated through resonance shifts into the high-frequency region of plate structures. As a result, substantial microwave absorption properties are expected for a hierarchical flower-like MoS_2 that is created from an extensive number of sheet-like units [16].

When a conductor is exposed to a time-varying magnetic field, circulating electrical currents, referred to as eddy currents, are induced within it. The magnitude of these currents varies with frequency, with substantial currents at lower frequencies, resulting in Joule heating and corresponding energy dissipation. However, as the frequency increases, the skin effect confines eddy currents to the conductor's surface, thereby minimizing their influence and the region through which they may flow. The fundamental framework for comprehending the behavior of eddy currents in conductive materials is provided by Faraday's Law. According to the skin effect idea, alternating currents, such as eddy currents, are limited to a smaller surface layer at higher frequencies, thereby reducing energy dissipation. A thorough understanding of this phenomenon is critical for analyzing eddy current behavior in high-frequency applications. Resonance at a specific frequency amplifies vibrations or currents within a structure, such as a plate, at that frequency. The magnitude of the generated eddy currents is reduced by shifting the resonance to higher frequencies, where the skin effect makes the eddy currents weaker. Higher frequency resonance shifts in plate structures minimize energy dissipation in conductive materials by increasing vibrational amplitudes and inhibiting eddy currents via the skin effect. The increase in inductive reactance and the reduction in eddy current resistance at higher frequencies limit current flow. This theory is often used in non-destructive testing methods and electromagnetic shielding. The amplification of unwanted eddy currents may be successfully reduced by shifting the resonance frequency of plate structures to higher bands, which is consistent with the approach of minimizing energy losses by resonance tuning.

This article offers a thorough synopsis of the developments in MoS_2-based materials in microwave absorption (MA). By discussing the microwave absorption (MA) traits of MoS_2 and its combinations, the study explored the most effective methods for improving the MA qualities of these composite materials. This review mainly focuses on studying the electromagnetic

characteristics of MoS_2, especially how the inclusion of composite materials with either dielectric or magnetic components, or both, affects those properties. Finally, we outline potential future paths and opportunities for MoS_2-based MAM development.

1.1 Structures and Properties of MoS_2

MoS_2 nanostructures are pretty different from those of other nanoparticles that are often classified as quantum dots (0D), one-dimensional (1D), two-dimensional (2D), or three-dimensional (3D) forms. Furthermore, its properties and potential applications vary according to the dimension, encompassing the possibilities of being metallic, superconducting, or semiconducting. It is present in several levels and forms. Its three possible bulk (3D) structures are rhombohedral (R), tri-agonal (T), and hexagonal (H), where 2H MoS_2 represents a two-layer hexagonal MoS_2. Three main features (1-T, 2-H, and 3-R) are identified in Figure 1. 1T is located in an octagonal configuration structure, while 2-H and 3-R are arranged in a trigonal prismatic shape [17]. Table 1 displays the lattice constants for every structure. It is established that the first structure is metallic, whereas the remaining two exhibit semiconducting properties [18]. Hexagonal MoS_2 monolayers also exhibit semi-conductivity properties. The 2-H and 3-R components function as arid lubricants as well. Because of its nonlinear optical properties, the 3-R phase finds applications in biomedical and nonlinear optical mass detection in quantum measurements [19]. Unlike other materials constrained to specific structural forms such as dots, wires, sheets, or bulk frameworks, MoS_2 exhibits a range of atomic configurations due to its structural adaptability. For example, MoS_2's many-phase materials might appeal to gas sensors that need rapid adsorption and high sensitivity [20]. Additionally, MoS_2's polymorphic structures show a 1H phase. The single-layer hexagonal configuration of the 1H phase is distinguished by the trigonal prismatic coordination of Sulphur atoms with molybdenum atoms. The electrical characteristics of MoS_2 are defined by this phase and others, such as the 2H and 1T phases: the 1H phase is semiconducting, while the 1T phase is metallic. Among the various crystalline forms of MoS_2, the 1T phase with an orthorhombic structure and the 2H phase with a hexagonal structure are the most common. The 1T phase is thermodynamically metastable and show metallic behavior, whereas the 2H phases are thermodynamically stable and shows semiconductor properties. In certain circumstances, the 1T and 2H phases may transform into one another [21]. In contrast to 2H-MoS_2, 1T-MoS_2 would exhibit greater conductivity and a wider layer spacing, which might significantly increase the sample's polarization intensity and, thus, its electromagnetic wave loss [22]. The attenuation and electrical conductivity of electromagnetic waves need to be further improved, despite MoS_2's powerful multiple scattering and reflection on electromagnetic waves. Additionally, preparing the 1T-MoS_2 metastable phase is challenging, which impedes further improvements to MoS_2's microwave absorption performance [23]. Weak van der Waals interactions keep neighboring monolayers apart and keep bulk MoS_2 monolayers together. Strong covalent Mo-S bonds exist inside each monolayer. It is typically present as black powder or particles. A MoS_2 monolayer is a structure comprising two S atom layers sandwiched between a Mo atom layer. The free spacing between MoS_2 monolayers is 0.30 nm, and the interlayer space is 0.62 nm [24]. The saturation S atoms on the bottom plane (apart from the edges) not only form individual MoS_2 monolayers but also chemically stabilize the bulk MoS_2 [25]. Depending on atom-stacking configurations, these monolayers may form either the trigonal prismatic 2H phase or the octahedral 1T phase. The temperature and flakes' thickness determine the conductivity of nanoMoS_2, which

rises with higher temperatures and falls with higher flakes' thicknesses until it approaches the bulk structure [26]. Furthermore, MoS_2 will unavoidably generate active sites throughout the preparation process, such as defects in structure or interfaces. Even if these flaws are just a few nanometers in size or even one atom, they will significantly alter the material's structure and electrical characteristics, impacting its usefulness [27]. The dielectric characteristics and microwave absorbing mechanism of MoS_2 could be effectively investigated. The application prospect of low-dimensional transition metal sulphide in the field of microwave absorption could finally be expanded if the microstructure of MoS_2 could be altered or designed in the real-world environment of two-dimensional materials and the structure-activity relationship of defects or interfaces could be introduced by means of qualitative characterization and analysis [28]. Additionally, single MoS_2 has low microwave absorption, which is why researchers are focused on exploring MoS_2 composite materials [29]. The microwave absorbance performance may be enhanced by composites made of magnetic or dielectric materials [30].

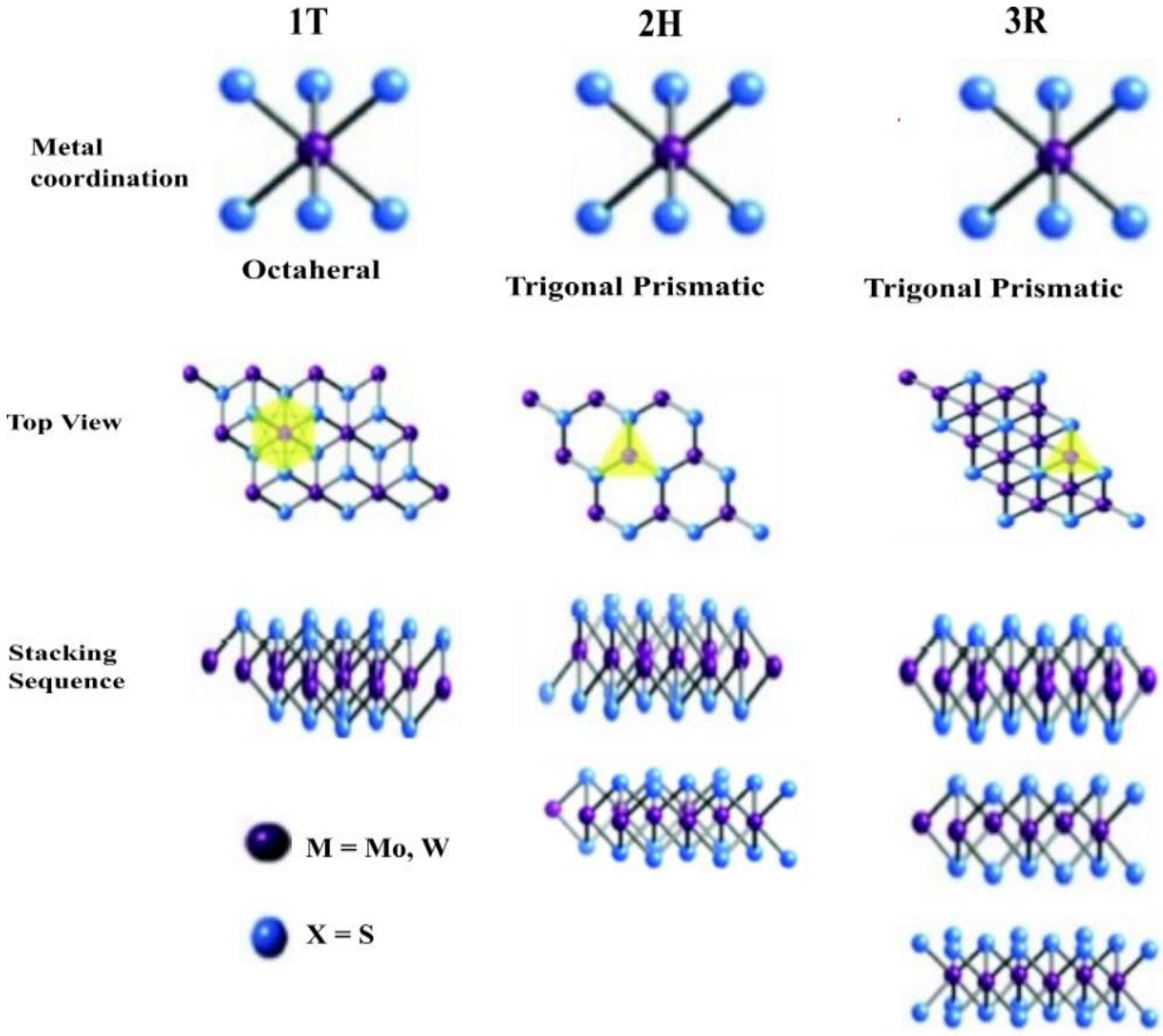

Figure 1 Distinct stacking and coordinating sequences for the MoS_2 structures 1T, 2H, and 3R [17].

Table 1 Comparison of several MoS_2 structures.

	1T	2H	3R
Composition of the structure	Octahedral	Trigonal prismatic	Trigonal prismatic
Properties of lattices	A = 5.60 Å, c = 5.99 Å and an edge sharing octahedral [31]	A = 3.14 Å, c = 12.30 Å [31]	A = 3.17 Å, c =18.38 Å [31]
Qualities	Both metallic and paramagnetic	Semiconductor	Semi-conductor
Electrical conductance	10^5 more than the phase of 2H	Low ($\approx 0.1 s/m$)	Low ($\approx 0.1 s/m$)
Peak of absorption	Peaks are absent at 604 nm.	Peaking between 604 and 667 nm	
Typical application	Chemical intercalation	Dry lubrications	Both non-linear optical devices and dry lubrication

Also, the metallic 1T phase of MoS_2 has a much lower charge transfer resistance than the semiconductor 2H and 3R phases, which makes it a much better conductor. In particular, 1T MoS_2 exhibits conductivity around 10^7 times greater than the 2H semiconducting phase [32]. Consequently, novel applications, including electrocatalysis, photocatalysis, supercapacitors, batteries etc., [33, 34] are made possible by the difference in conductivity between 1T and 2H-phase MoS_2. Interestingly, the multiphase 1T/2H-MoS_2 can acquire both semiconductor and magnetic properties by incorporating magnetic 1T-MoS_2 into semiconducting 2H-MoS_2. In other words, 1T-phase-incorporated 2H-MoS_2 nanosheets can produce room-temperature magnetization behavior in non-magnetic 2H-MoS_2 semiconductors [35]. Therefore, researchers anticipate that it will be a successful method of refining the electromagnetic properties of MoS_2 and a fresh approach to modifying the absorbance of microwaves in MoS_2-based absorbers.

2. Microwave Absorption Mechanism of Materials Based on MoS_2

There are usually two processes involved in the material's microwave absorption process. First, microwaves completely penetrate the absorber. Permittivity and permeability are necessary for this procedure to meet the impedance matching requirement [36]. Subsequent conversion and dissipation of the microwave energy penetrating the absorber are associated with the material's internal loss process. Magnetic and dielectric losses are the primary loss mechanisms [37].

2.1 Process of Microwave Absorption and Attenuation

According to Maxwell's electromagnetic field theory, changes in the magnetic field induce changes in the electric field, while an ever-changing electric field causes a constantly varying magnetic field. Consequently, altering magnetic and electric fields mutually induce each other, generating synchronized waves propagating from nearby to distant regions at a specific velocity. This process gives rise to the generation of electromagnetic waves [38]. When electromagnetic

waves come into contact with a solid material, various interactions take place, including absorption, reflection, secondary reflection, transmission, and retransmission. Absorption, reflection, and transmission are the three EM response behaviors that occur when a two-dimensional (2D) material is used instead of a bulk material [39]. Additionally, retransmission and secondary reflection disappear. Figure 2 shows a comparison between 2D materials and solid bulk materials [40]. Furthermore, certain 2D materials, like $Ti_3C_2T_x$, possess a layer-by-layer developed structure, which may lead to numerous reflections and scattering in addition to being advantageous for microwave absorption and attenuation. According to optical laws, electromagnetic waves are reflected, absorbed, and transmitted when they strike absorbing materials' surfaces. The conduction and displacement currents are the two distinct electrical currents that arise inside a non-magnetic dielectric material when electromagnetic waves strike its surface. Most charge carriers do not participate in the process of conducting dielectric materials. Because of this, the bonded charges may be shifted if the material is exposed to an extra electrical field [41]. Through a process known as polarization, displacing these electrical charges may result in the creation of a dipole field, which is the equivalent applied field. The dielectric tangent is the tangent of the angle at which the displacement phasors and the total current form. These bonded charges result in the displacement of electrical current, while a net flow of free charges produces the conductive current. For 2D materials, it is essential to measure the attenuation functions and one-layer electromagnetic wave responses. The incident waves are converted into transmission waves (T), absorption waves (A), and reflectance waves (R), as shown in Figure 2(a). The absorbing properties of a single-layer 2D material may be affected by high electrical conductivity, which converts electromagnetic waves into electrical energy, and polarization loss, which converts electromagnetic waves into thermal energy Figure 2(b) [42]. The dielectric loss may considerably attenuate and absorb waves in 2D materials like graphene. Both internal and extrinsic losses are included in the dielectric loss. The former is dependent on the material's crystal structure. The microstructure's defects, including microcracks, porosity, uneven crystalline orientation, and grain boundaries, are associated with extrinsic loss [43, 44]. The relaxation and conduction losses, which are mostly influenced by the material's conductivity and polarisation, respectively, are included in the dielectric loss [45]. Polarisation generally results from certain functional groups, imperfections, and interfaces. Furthermore, intrinsic and hopping conduction are the two key factors influencing electrical conductivity; despite its low conductivity, the hopping conduction mechanism probably has the most impact [46].

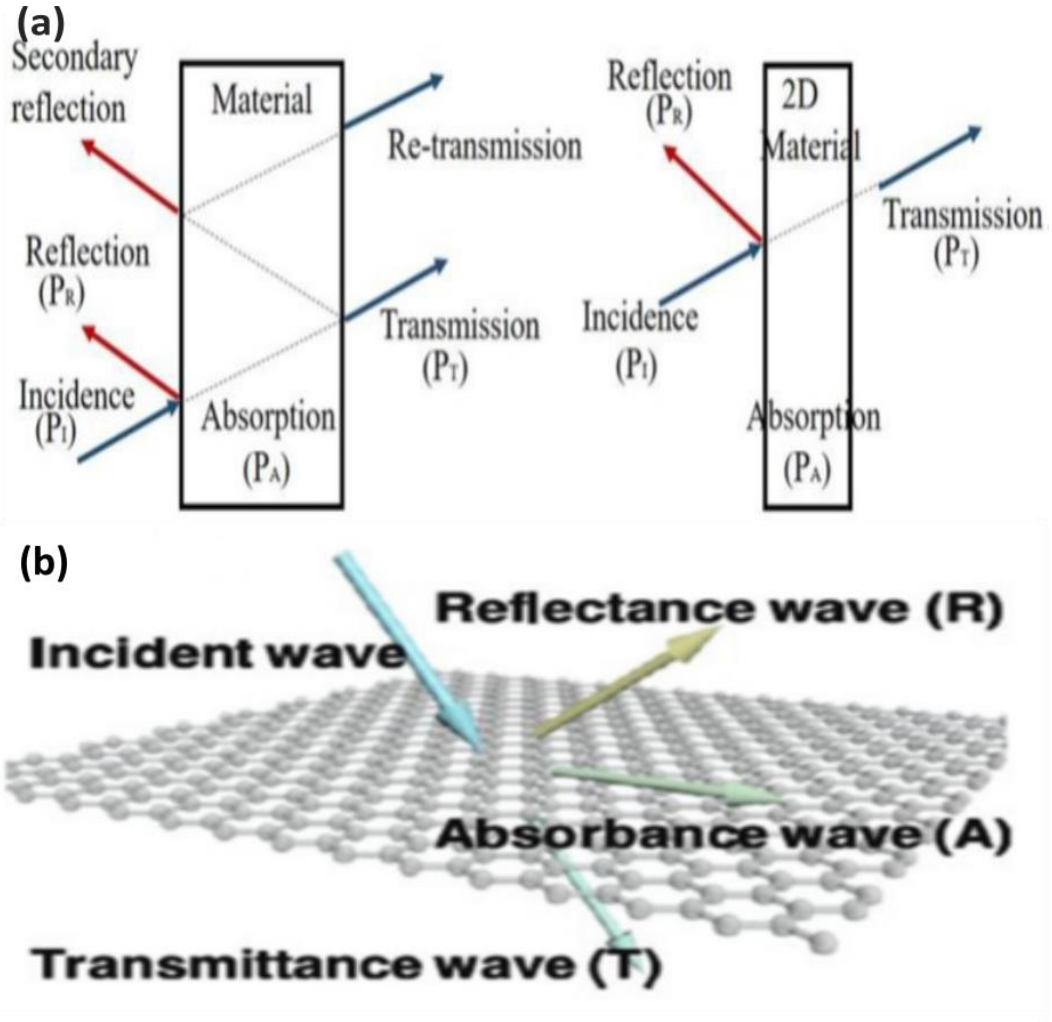

Figure 2 Illustration of the incidence of electromagnetic waves (EM) through two types of materials: (a) solid and two-dimensional; (b) single-layer [47].

2.2 Theories of Microwave Absorption

The electromagnetic wave will follow three distinct processes when it enters the material's surface: transmission, absorption, and reflection [48]. The mismatch in the incident medium's surface impedance is the primary cause of electromagnetic wave reflection. The more electromagnetic waves are reflected, the greater the impedance difference between the surfaces. The inherent electromagnetic loss characteristics of the material determine how the incoming electromagnetic wave is absorbed. Attenuation constant (α), complex permeability (μ_r), and complex permittivity (ε_r) are often used to characterize a material's loss properties. Consequently, impedance matching and attenuation characteristics are two essential requirements that must be met to optimize the absorption of electromagnetic waves [49].

2.2.1 Impedance Matching

Enhancing an appropriate matched impedance between the incident wave and the absorbing substance at the interface within free space is critical to improving the entrance of electromagnetic waves into the substance. This factor, referred to as impedance matching characteristics, is essential

[49]. Achieving perfect impedance matching is the primary factor determining how effectively the material absorbs an electromagnetic wave since it may only be lost once it enters the substance. When an electromagnetic wave (EM wave) propagates through a vacuum with impedance Z_0 and reaches the surface of a losing medium with an input impedance Z_{in}, it may encounter both transmission and reflection. A matched impedance is a vital component that determines the amount of electromagnetic wave transmission. One might compute the impedance matching degree (|Δ|) using equation (1) [50]:

$$|\Delta| = |sinh^2(Kfd)\text{-}M| \tag{1}$$

Properties of permittivity's and permeabilities may be used to calculate the values of two variables, M and K.

$$K = \frac{4\pi\sqrt{\mu'\varepsilon'}sin\left(\frac{\varepsilon''/\varepsilon'\,\mu''/\mu'}{2}\right)}{c\cdot cos(\varepsilon''/\varepsilon')cos(\mu''/\mu')} \tag{2}$$

$$M = \frac{4\mu'\varepsilon'\cdot cos(\varepsilon''/\varepsilon')\cdot cos(\mu''/\mu')}{\left(\mu' cos(\varepsilon''/\varepsilon') - \varepsilon' cos(\mu''/\mu')\right)^2} + \left[tan\frac{\varepsilon''/\varepsilon' - \mu''/\mu'}{2}\right]^2 \left(\mu' cos(\varepsilon''/\varepsilon') + \varepsilon' cos(\mu''/\mu')\right)^2 \tag{3}$$

In this case, ε' and ε'' stand for the real and imaginary components of ε_r, while c is the speed of light in a vacuum. μ' and μ'' also stand for the real and imaginary portions of μ_r. Successful impedance matching is shown when the magnitude of Δ is close to zero for a given thickness. If it differs much from zero, impedance matching is considered insufficient. Furthermore, interferometric phase elimination may also reduce electromagnetic waves at specific wavelengths. In other words, absorbers may, under certain boundary circumstances, attenuate incoming electromagnetic waves. When the layer thickness d of the absorbing material corresponds to an odd integer of $\left(\frac{1}{4}\right)$λ of the incoming wave, the electromagnetic wave with a given frequency will be reflected [51]. Moreover, coherent destructive interference will be used to cancel out the waves. Equation (4) illustrates the quarter-wavelength wave theory [52]:

$$\mathrm{d} = \left(\frac{n}{4}\right)\lambda_0/(|\varepsilon_r||\mu_r|)^{\frac{1}{2}}(\mathrm{n} = 1,3,5,7\ldots) \tag{4}$$

Here, 'd' represents the layer thickness, 'f' for the equivalent frequency, and 'c' is the speed of electromagnetic radiation in a vacuum. The phase difference between the absorbing layer's surface and bottom may vary by changing the thickness. If the phase difference is an odd multiple of the half wavelength, the two waves have opposing phases. In this case, their mutual interference will successfully neutralize one another, resulting in the desired reduction of electromagnetic waves.

2.2.2 Attenuation Characteristics

The majority of electromagnetic waves may penetrate a material once the absorbing material and the impedance-matching concept come into contact. To minimize the emission of electromagnetic waves, it's crucial to depend on the intrinsic properties of the material described by $\varepsilon_r = \varepsilon' - j\varepsilon''$ and $\mu_r = \mu' - j\mu''$, which signify the material's loss characteristics. The real parts

of permittivity's and permeabilities represent a material's ability to preserve electrical and magnetic energies, while the imaginary parts represent a material's ability to dissipate electromagnetic energies, respectively. Therefore, ε'' and μ'' are essential factors in determining how well EM waves attenuate [52]. Materials' loss capacity may be calculated using the tangent of dielectric losses and the magnetic losses tangent, which are shown in equations 5 and 6.

$$tan\delta_{\varepsilon} = \frac{\varepsilon''}{\varepsilon'} \tag{5}$$

$$tan\delta_{\mu} = \frac{\mu''}{\mu'} \tag{6}$$

According to theory, a material's ability to reduce electromagnetic energy rises as its electromagnetic loss tangent and dielectric loss tangent values rise. On the other hand, expanding ε'' and μ'' arbitrarily would increase the impedance matching degree and negatively impact absorption capacity overall.

Several parameters should be carefully considered in practical applications to develop microwave-absorbing materials that satisfy the needs of "thin, lightweight, wide-bandwidth, and strong absorption" [53]. The electromagnetic parameters must meet specific requirements for the material to have the necessary attenuation qualities. Equations (7) and (8) may be used to calculate the reflection loss (RL), which is a standard method of determining a material's absorbent capacity [54].

$$\mathrm{RL} = 20\log\left|\frac{Z_{in} - Z_0}{Z_{in} + Z_0}\right| \tag{7}$$

$$Z_{in} = \sqrt{\frac{\mu_r}{\varepsilon_r}}\tanh\left[j\left(\frac{2\pi f d}{c}\right)\sqrt{\mu_r\varepsilon_r}\right] \tag{8}$$

$$Z_0 = \sqrt{\frac{\mu_0}{\varepsilon_0}} \tag{9}$$

In this context, Z_{in} corresponds to the input impedance of the absorbing material, Z_0 represent the free space impedance 'd' signifies the thickness of the specified material, 'C' represents the speed of light, and 'f' denotes the given frequency. The better a substance absorbs electromagnetic radiation, the higher its RL value. Effective absorption is 90% absorption when the RL value is less than -10 dB. The term "effective absorption bandwidth" (EAB) refers to the frequency range that an absorbent might effectively absorb. Apart from the RL value, the attenuation coefficient (α) may also be used to express the material's ability to attenuate electromagnetic waves in accordance with the microwave transmission principle. Equation (10) is used to calculate this coefficient [55].

$$\alpha = \left(\sqrt{2\pi f}/c\right) \times \sqrt{(\mu''\varepsilon'' - \mu'\varepsilon') + \sqrt{(\mu''\varepsilon'' - \mu'\varepsilon')^2 + (\varepsilon'\mu'' - \varepsilon''\mu')^2}} \tag{10}$$

Here, c denotes the electromagnetic wave's velocity in a vacuum, while f signifies the frequency of the incident wave. Theoretically, a material's ability to attenuate electromagnetic waves

increases with its α value. In conclusion, the ability of a material to absorb electromagnetic waves is determined by its attenuation and impedance matching characteristics; often, the RL value is used to measure the absorption efficiency of the material.

2.3 Losses Mechanism

2.3.1 Magnetic Loss

The energy used by ferromagnets to resist the coercive force when magnetized within a magnetic field is commonly known as hysteresis loss in magnetic materials [56]. As a result, the intrinsic coercive strength of the magnetic material itself will influence its hysteresis loss [57]. Additionally, the term "eddy current loss" describes the energy dissipation produced by the eddy current when magnetic materials are electromagnetically inducted under an alternating magnetic field [58]. Furthermore, there is residual magnetism because the magnetic flux density changes more slowly than the applied magnetic field. The magnetic flux density of the internal magnetic material and the applied magnetic field are unequal [59, 60]. Therefore, the residual loss is the energy loss produced to remove the remaining magnetic [61]. Furthermore, the resonance created by the magnetic material absorbing a significant quantity of energy from the surrounding electromagnetic field in order to preserve the stability of the interior magnetic flux density is known as natural resonance [62]. A specific vibration will take place at the magnetic domain wall of the magnetic substance as a result of the force received and the action of the magnetic field [63]. The domain wall will shake and suffer a specific loss when the vibration frequency matches the frequency of the external magnetic field. Exchange resonance produces a relaxation loss at the highest and ultrahigh frequencies [64].

Magnetic metals are often used in microwave absorption applications because of their relatively high saturation magnetization, which enhances permeability and is consistent with the Snoek limit [65]. However, at higher frequencies, their high electrical conductivity reduces permeability [66]. A practical approach for achieving enhanced microwave absorption properties (MAPs) involves leveraging the cooperative interaction between magnetic metals and MoS_2. Ferromagnetism in the non-magnetic semiconducting MoS_2 may be produced by cation doping or by introducing a metallic 1T phase into semiconducting 2H-MoS_2, according to theoretical predictions and experimental investigations [67]. Large saturation magnetization, complex permeability, and eddy current loss-especially from natural and exchange resonances-are characteristics of magnetic materials that effectively absorb microwaves by magnetic loss [68]. A highly effective approach to enhancing microwave absorption through combined magnetic and dielectric loss mechanisms is the integration of MoS_2 with magnetic nanostructures [69]. To maximize impedance matching and improve microwave attenuation, magnetic nanostructures may introduce magnetic losses into MoS_2-based systems and provide a synergistic effect. Magnetic materials are classified as metal oxides (spinal ferrites and hexagonal ferrites) and metals/alloys (Fe, Co, Ni, FeCo, and FeNi) based on their chemical makeup and structure. This variety offers a wide range of magnetic property adjustments to customize its microwave-absorbing performance. The synthesis, structure, and microwave absorption characteristics of MoS_2@magnetic material composites are covered in the sections that follow.

The in-situ development of magnetic metals on MoS_2 nanosheets promotes the production of magnetic-dielectric structures, which boost absorption performance via combined magnetic and dielectric features. One of the primary research studies in the field of electromagnetic (EM) wave

absorption is the creation of composite materials that incorporate MoS_2 along with magnetic components [70]. One important metric that describes an object's capacity to produce a magnetic field in a certain orientation is its magnetic moment, which measures the substance's magnetic intensity and the direction of its magnetic field [71].

Wang et al. (2019) report that the magnetic properties of MoS_2 are generally enhanced when combined with metal oxides. Specifically, the saturation magnetization of MoS_2 increased from 0.53 $emu \cdot g^{-1}$ for undoped MoS_2 to 0.93 $emu \cdot g^{-1}$ upon doping with 3% nickel (Ni). The zigzag edges and changes in the quantity of voids in the material might cause this improvement. The synthesized nanocomposite achieved a maximum reflection loss of -58.08 dB at an optimal thickness of 2.05 mm [72]. 2D MoS_2 may acquire a magnetic moment by transition metal doping. Numerous recent investigations have demonstrated that incorporating transition metal elements into MoS_2 may result in magnetically active materials. For example, Schwingenschlögl et al. [73], computed the stability and magnetic characteristics of monolayer MoS_2 doped with IV, V, and VI transition metals using density functional theory (DFT). Their results showed that single Mn, Fe, Co, or Zn atoms may be used to replace Mo atoms in MoS_2 to create diluted magnetic semiconductors. The stability and electromagnetic characteristics of monolayer MoS_2 doped with V, Cr, Mn, Fe, and Co were examined in further detail by Yue et al. [74], who confirmed that these hybrid MoS_2 structures show notable stability.

Remaining losses, hysteresis/looping losses, and eddy current losses are the main methods for attenuating microwave radiation that leads to magnetic losses [14]. The term "eddy current loss" describes the material in the oscillating high-energy electromagnetic field as a result of eddy currents being electromagnetically induced. Figure 3(a) shows the contribution of Magnetic Loss Mechanisms for microwave absorption. To investigate the eddy loss process, the eddy current loss coefficient C_0 [75] is computed using the equation 11:

$$C_0 = \mu''(\mu')^{-2}\mathrm{f}^{-1} = 2\pi\mu_0 d^2\delta \tag{11}$$

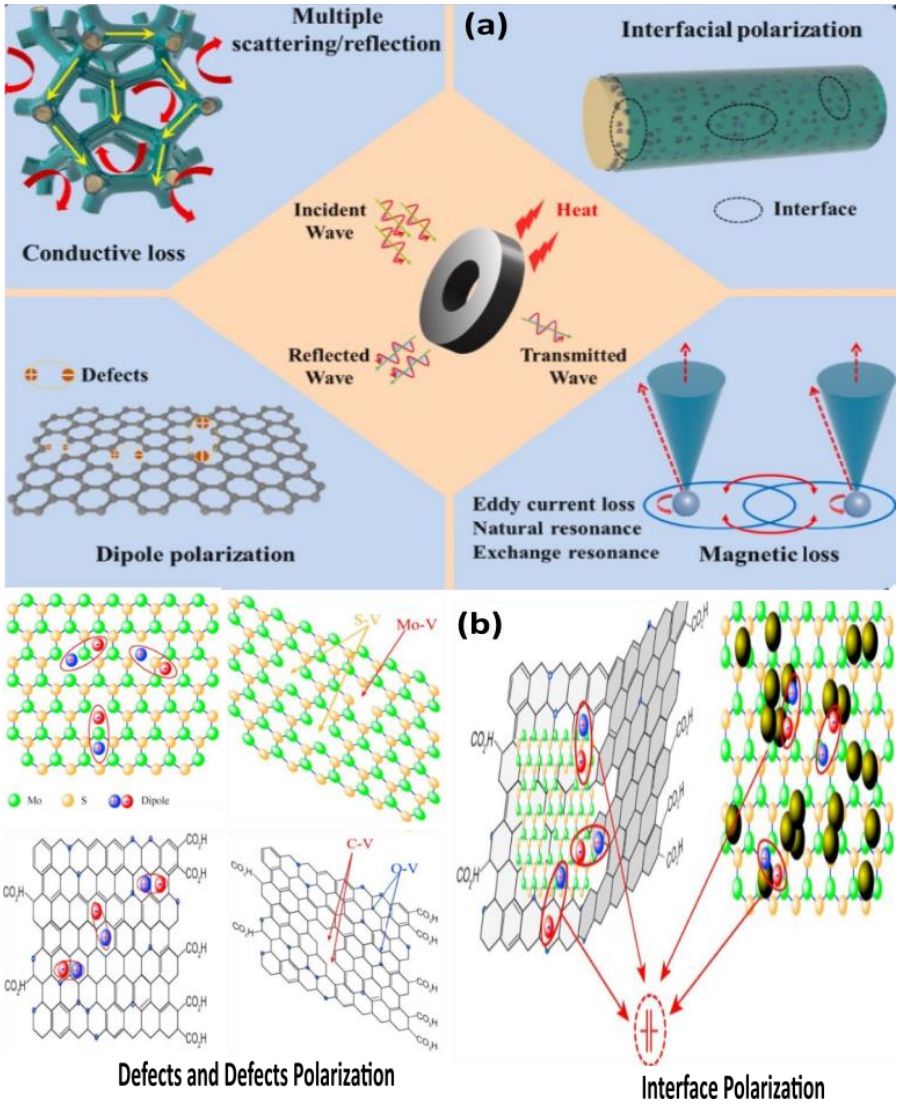

Figure 3 Microwave absorbing performance of MAMs showing the contribution of (a) Losses Mechanisms and (b) Polarisation Defects [76, 77].

Where f is the frequency, d is the absorber's thickness, δ represents the conductivity, μ' represents the permeability's real component, μ'' is its imaginary part, and μ_0 is the vacuum permeability [78]. The measured real and imaginary components of permeability may be substituted into Equation 10 to get the value of C_0 [79]. In general, it is possible to determine whether eddy loss or natural resonance loss is responsible for the material's magnetic loss by observing how the value of C_0 changes with frequency [80]. Natural resonance loss is the primary source of the material's magnetic loss if the C_0 value curve exhibits significant frequency fluctuations. Conversely, the eddy current loss is the primary source of the material's magnetic loss if the value of C_0 is almost constant [81].

This phase inconsistency between the magnetic field and induction causes the microwave energy to dissipate as thermal energy. Hysteresis loss occurs in magnetic materials due to irreversible magnetization phenomena such as domain wall displacement and rotation. Residual losses, on the other hand, result from a variety of mechanism-driven magnetization relaxation processes [82]. The magnetization relaxation process causes permeability's real and imaginary components to vary with frequency. When electrons and ions are out of equilibrium, magnetic hysteresis plays a significant

role in the residual loss at low frequencies and weak magnetic fields. The bulk of the residual loss at high frequencies comprises domain wall resonance, dimensional resonance, and natural resonance. Figure 3 illustrates polarisation defects, magnetic loss mechanisms, and multiple scattering for MAMs.

2.3.2 Electrical Conduction Loss

Some carriers will continue to undergo directional drift under the operation of the microwaves since the accurate absorption medium is not a perfect insulator, which will result in the generation of a conduction current. The joule heat created by this electric current leads to the dissipation of microwave energy due to its thermal effect. The material's electrical conductivity affects this dissipation process. This process generally accounts for a large fraction of the behavior in high-conductivity materials [83]. MoS_2's special structure helps build conductive networks when paired with conductive materials. These networks allow polarized electrons to migrate and jump between neighboring sites, resulting in excellent conductivity for microwave attenuation. Figure 3(b) illustrates the microwave behavior and loss mechanism for MAMs.

2.3.3 Loss as a Result of Polarisation Relaxation Defects and Defects Polarization

Polarisation is produced when a medium has asymmetric positive and negative charges in the presence of an electric field. Regarding composite component media, the Maxwell-Wanger effect-also referred to as interface, dipole, and defect-induced polarisation in the microwave frequency range-is the primary cause of the medium's polarisation [76]. Electromagnetic energy is transformed into other kinds of energy by the polarisation relaxation and damping processes that follow since polarisation cannot keep up with the frequency shift of the external electric field. Polarisation often encompasses many methods, including dipole, interface, atomic, and electron polarisation as shown in Figure 4. When carrier movement at the material interface is impeded and turns into a bound charge that develops within the contact, interfacial polarisation often occurs in the low-frequency region.

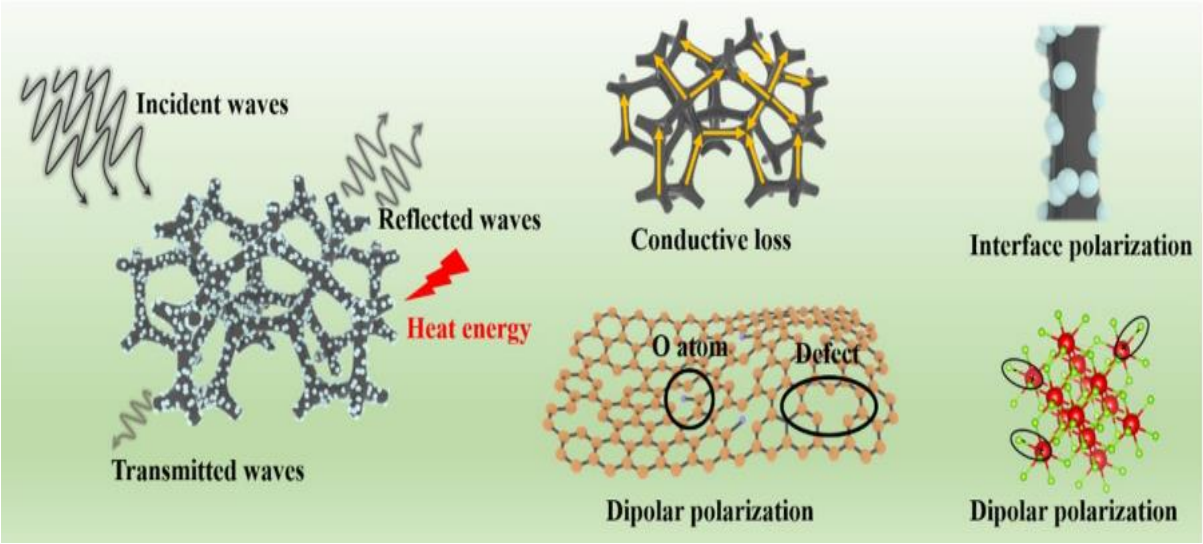

Figure 4 Schematic representation of various polarization mechanisms in microwave absorbing materials (MAMs).

The real component of the material's permittivity will rise as a result of the charge aggregation-induced field distortion. The primary polarisation mechanism in the gigahertz region of microwave frequencies is dipole polarisation. When an electromagnetic field is introduced, the originally disorderly configuration of dipoles will spin with a constant orientation and alter in response to the introduction of an electromagnetic field. Permittivity is affected by the relaxation process that often occurs along with dipole polarisation. Debye models may generally be used to examine the medium's relaxation process. The Havriliake-Negami dielectric polarisation relaxation relation yields the following formula [84]:

$$\left(\varepsilon' - \frac{\varepsilon_s + \varepsilon_\infty}{2}\right)^2 + (\varepsilon'')^2 = \left(\frac{\varepsilon_s - \varepsilon_\infty}{2}\right)^2 \quad (12)$$

In this context, ε_s stands for the stationary permittivity, ε_∞ represents the comparative dielectric permittivity at higher frequencies, ε' denotes the real permittivity and ε'' represents the imaginary permittivity. When Debye relaxation behavior is present, the medium's ε' and ε'' plots will resemble a semicircle, sometimes referred to as a Cole-Cole semicircle. Each semicircle represents a Debye relaxation process [85].

2.3.4 Dielectric Losses

In comparison to traditional carbon-based dielectric absorbers, the dielectric-dominated MoS_2 sheet absorbent for EMW absorption was initially demonstrated in 2015 and showed higher attenuation performance. Defect dipole polarisation from Mo and S vacancies, together with the nanomaterial's larger specific surface area, were credited with improved microwave absorption [86]. In microwave absorption, relaxation polarisation and conduction loss are the most frequent dielectric losses [87]. Any dielectric substance will create a leaky conduction current when exposed to an electric field, but this current will dissipate as heat, causing conduction loss [88]. Moreover, the current flowing through the material due to the dielectric's relaxation polarisation is what causes the relaxation polarisation loss [89]. The Debye relaxation theory ought to be the most popular and developed of the dielectric polarization theories. The real and imaginary parts of a material's permittivity are not independent, in accordance with Debye's relaxation theory, and they have a connection like this (Eqn.11) [90]. Consequently, Cole-Cole curves at various frequencies or temperatures are the graphs that show the connection between the real and imaginary sections of the permittivity [91]. A semi-circle is comparable to the Cole-Cole correlation because of the conductivity loss inside the material [92]. Polarisation loss would be the primary source of the loss at this point, with each semicircle representing a relaxation polarisation process [93]. On the other hand, conductive loss could be the primary cause of losses if the Cole-Cole relation is a sloped straight line. Liang created 2D MoS_2 nanosheets using a straightforward hydrothermal process in 2016 in order to investigate their microwave absorption characteristics. The findings showed that the MoS_2 nanosheets' high dielectric loss and improved interfacial polarization made them very efficient electromagnetic (EM) absorbers [94].

3. Method of Synthesis of MoS_2

There are two ways to synthesize nanostructured MoS_2: top-down and bottom-up. Using a top-down method, commercially available MoS_2 bulk crystals are physically reduced to MoS_2

nanoparticle size [95]. In contrast, the bottom-up method uses hydrothermal or solvothermal techniques, chemical vapor deposition (CVD), and other small-molecule reactions to synthesize MoS_2 nanomaterials [96]. Furthermore, research has been published on MoS_2 monolayers, multiple layers, nanoparticles, and quantum dots [97]. In both top-down and bottom-up approaches, ongoing attempts have been documented to fabricate MoS_2 nanomaterials [98, 99]. Figure 5 shows different synthesis techniques for producing MoS_2.

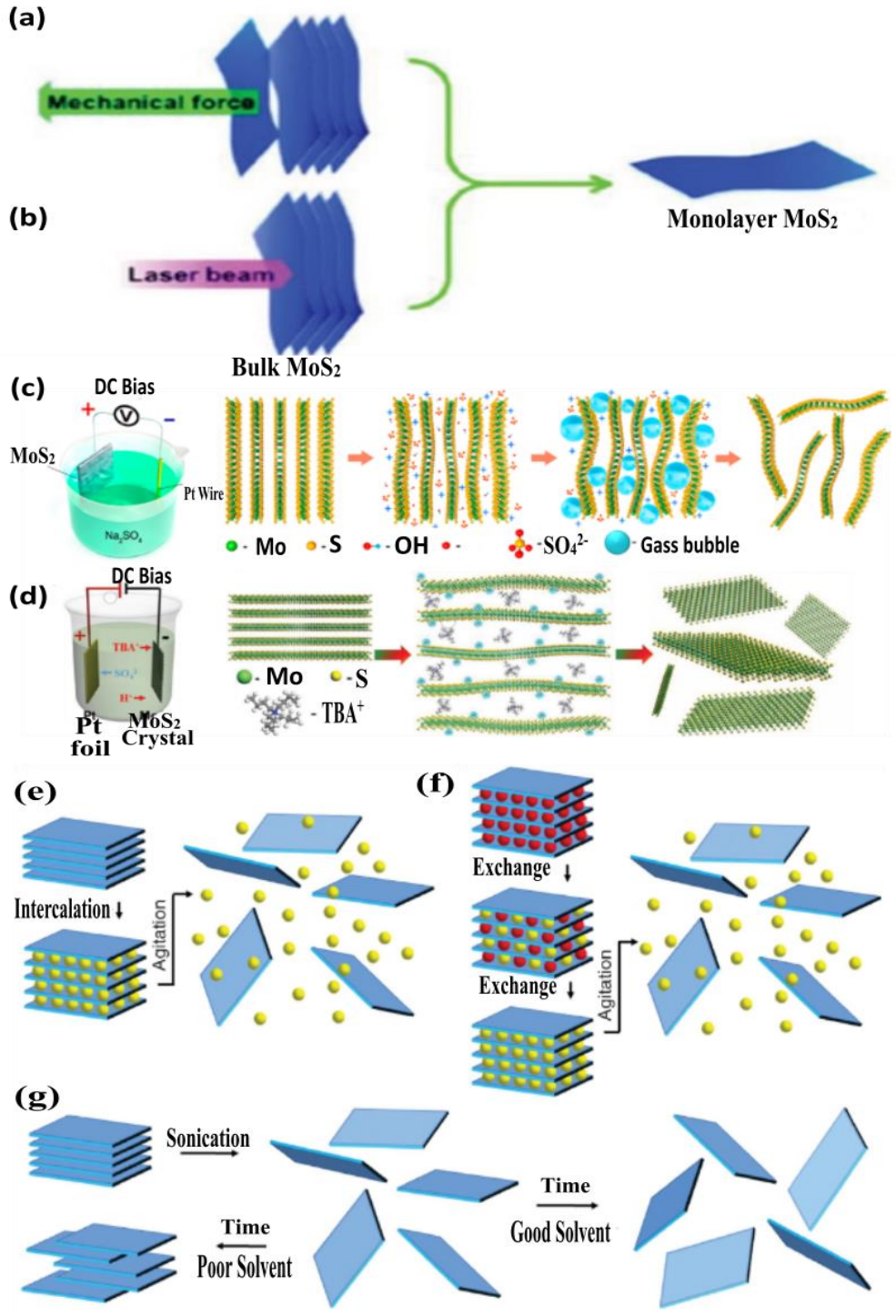

Figure 5 Schematic representation of the mechanisms for (a-b) mechanical and laser exfoliation, (c) anodic and (d) cathodic electrochemical exfoliation of MoS_2 nanosheets (e-g) main liquid-phase exfoliation [100-103]. Bulk MoS_2.

3.1 Top-Down Method

3.1.1 MoS_2 Exfoliation

The exfoliation approach may readily generate MoS_2 nanosheets because of the multilayered structure and van der Waals interactions. MoS_2 nanosheets have been synthesized via liquid-phase exfoliation, chemical exfoliation, mechanical exfoliation, and electromechanical exfoliation, as described [104, 105]. For instance, in the mechanical exfoliation method, appropriate MoS_2flakes are delicately separated from the bulk MoS_2 crystal using adhesive tape and then transferred onto a designated substrate [106]. When the scotch tape is taken off, some MoS_2 remains on the substrate. Consequently, random-shaped and sized single- or few-layer MoS_2 nanosheets are produced. The exfoliation approach produces high-quality 2D materials that are useful for studying the purity of materials and device performance. Nevertheless, it is challenging to regulate the MoS_2's thickness and size during this process, and the materials that are produced are unsuitable for large-scale manufacturing and scaled-up applications [107]. Li et al. [108], used the sticky tape approach to physically exfoliate monolayer- and multilayer MoS_2 nanosheets from SiO_2/Si. MoS_2 flakes were mechanically separated from their substrate, Si/SiO_2. An atomic force microscope (AFM) and a bright-field optical microscope were used to characterize the single-layer and multilayer MoS_2 materials. AFM investigations showed that the height of a single MoS_2 sheet was 0.8 nm, while the thicknesses of 2, 3, and 4 layers of MoS_2 nanosheets were 1.5, 2.1, and 2.9 nm, respectively. It was discovered that the van der Waals connections between MoS_2 and SiO_2 were significantly weakened. Because of its significant affinity for Sulphur, gold may be used as a substrate to exfoliate the MoS_2 nanosheets for this purpose. Owing to the powerful van der Waals connections between the Au and MoS_2 layers, gold can effectively separate the MoS_2 monolayer from the bulk material [109, 110]. Huang et al. [111] used an Au-assisted exfoliation technique to create large-area MoS_2 nanosheets. A Ti or Cr adhesion-coated substrate was covered with a thin layer of Au in a conventional synthesis. It is necessary to pass a MoS_2 bulk crystal under high pressure in order for it to make excellent contact with an Au-covered substrate on tape. The large-area monolayer sheets were recovered from the Au surface when the tape was removed. Top-down methods are utilized to create single- and multilayer MoS_2 nanosheets, which have been used to study some of the fundamental properties of MoS_2 nanosheets.

3.1.2 Mechanical Exfoliation

One popular technique for creating MoS_2 nanomaterials is mechanical exfoliation, which is well-recognized for separating bulk material from thin, highly crystallinity-rich layers. This technique was first developed using sticky tape and is perfect for study since it successfully maintains the crystal structure of MoS_2. This technique, which involves using adhesive tape to remove thin MoS_2 sheets from a block of MoS_2, is also known as micro-mechanical exfoliation. Frindt et al. [112] initially introduced this technique in 1965, and it was effective in obtaining a large number of layers of MoS_2. Mechanical exfoliation remains the most effective technique for producing the purest, most crystalline, and precisely thin nanosheets from layered materials to date [113]. Despite the high degree of crystallinity of MoS_2 produced through this approach, large-scale applications remain challenging due to the inefficiencies and lack of reproducibility in the preparation process. Consequently, researchers have investigated ultrasound-assisted exfoliation techniques. Utilizing 1-

Dodecanethiol, Liu et al. [114] successfully synthesized graphene-like MoS_2 materials via ultrasonic exfoliation (Figure 5a). The highest concentration of graphene-like MoS_2 was accomplished when the volume ratio of 1-dodecanethiol to trichloromethane was 1:1, and the ultrasonication duration was maintained at 12 hours. Additionally, dual-solvent ultrasonic exfoliation was facilitated by incorporating chloroform Bulk crystals, which were pushed onto 3M scotch tape and folded several times in the conventional mechanical exfoliation dichalcogenides (TMD) process (Figure 5b). To ensure that the tape containing the MoS_2 samples adheres effectively to the substrate, an appropriate amount of pressure is applied. Upon removal of the Scotch tape, the surface of the SiO_2/Si substrate is coated with numerous TMD flakes. This technique can yield nearly all high-quality monolayers of two-dimensional TMDs [115]. Radisavljevic et al. utilized this technique in 2011 to exfoliate monolayer MoS_2, which was employed as the channel material in the fabrication of an interbond tunneling field-effect transistor (FET) [116]. This kind of transistor uses less power than conventional transistors. The development of applications for 2DTMD single crystals is hindered by a significant limitation of the conventional mechanical exfoliation (ME) method, which yields small crystal sizes ranging from tens to hundreds of microns, along with a low yield and the potential for adhesive residue [117]. To address these challenges, several modified ME techniques have been developed to produce monolayer TMD crystals.

3.1.3 Electrochemical Exfoliation

Electrochemical exfoliation of MoS_2 is an effective technique for generating high-quality nanosheets suitable for microwave absorption applications. The resultant materials exhibit increased surface area and tunable electromagnetic properties, rendering them ideal candidates for diverse technologies in microwave engineering and materials science. Future research efforts may optimize exfoliation conditions and investigate hybrid materials to further improve microwave absorption efficiency [118]. Electrochemical exfoliation has been reported to produce MoS_2 nanoflakes in their pure 2H phase without altering their intrinsic structure. This contrasts with the commonly used chemical exfoliation and hydrothermal synthesis methods for nanoscale MoS_2 production, which tend to facilitate the formation of the 1T phase [119]. Techniques for producing MoS_2 nanosheets via electrochemical exfoliation can be categorized into anode exfoliation, cathode exfoliation, and other electrochemical exfoliation methods, depending on the configuration of the exfoliation electrodes. Anode exfoliation is performed using diluted H_2SO_4 [120] or Na_2SO_4 [121] solution with bulk MoS_2 as the anode and platinum wire or foil as the cathode. The procedure is comparable to graphene exfoliation by anode [122]. The oxidation of electrolyzed water generates oxygen-containing radicals (OH and O) that congregate around sizable MoS_2 crystals when a voltage is applied to the working electrode material. The dW force between the two layers is weakened when intercalated $SO4^{2-}$ enters the gap between the MoS_2 layers as a result of the oxygen radicals attacking the edges of the bulk MoS_2 crystals. Moreover, the distance between layers of MoS_2 is further increased by the emission of O_2 produced by oxygen-containing free radical oxidation and SO_2 gas produced by sulphate ion reduction.

Ultimately, the gas's eruption force separates the 2D MoS_2 flakes from the main MoS_2 crystal, leaving them floating in the electrolyte (Figure 5b) [100]. The two primary components for achieving anodic exfoliation are the generation of gases and oxygen-containing free radicals. In contrast to anodic exfoliation, cathodic exfoliation is employed to produce MoS_2 nanosheets using bulk MoS_2

crystals as cathodes and platinum wires or foils as anodes, either in an aqueous solution of inorganic salts (such as (K_2SO_4 or KCl)) or in an organic solution of long-chain ammonium salts. This exfoliation's mechanism and procedure are comparable to those of graphene's electrochemical cathode exfoliation. Tetra-n-butylammonium bisulfate ($TBA.HSO_4$) is a common example of cathodic exfoliating bulk MoS_2. Zhang et al. employed it in propylene carbonate as an electrolyte to create 2D MoS_2 flakes by cathodic electromechanical exfoliation [101]. When voltage is applied, the TBA^+ cation ($TBA \cdot HSO_4 \rightleftharpoons TBA^+ + HSO_4^-$) intercalation penetrates the negative charged MoS_2 crystal interlayer and causes the interlayer distance to increase to 0.89 nm. Hydrogen bubbles are then created by the migration and reduction of H^+ ions ($HSO_2^- \rightleftharpoons SO_4^{2-} + H^+$, $2H^+ + 2e^- \rightarrow H_2$), which widens the space between neighboring layers even more. Ultimately, under the influence of gas eruption, the MoS_2 nanosheets are separated and suspended in the electrolyte. Thus, the primary criteria for accomplishing cathode exfoliation are the choice of an appropriate electrolyte to accomplish the intercalation of cathode ions and the production of gas (Figure 5c). In addition, the development of unstable 2H-MoS_2 due to the oxidation of the anode exfoliation is prevented since the cathode exfoliation is mostly conducted in an organic solvent. include the use of organic solvents and electrolytes. The process is simple to use and safe for the environment. Therefore, it is anticipated that this technique will be used to exfoliate MoS_2 on a wide scale. You et al. (2014) demonstrated how to create single-layer or multiple layers of nanosheets of MoS_2 (with lateral sizes up to 20 μm) in a diluted H_2SO_4 electrolyte through anodic exfoliation. During this process, oxygen free radicals and SO_4^{2-} ions intercalate into bulk MoS_2 crystals, generating SO_2 or O_2 bubbles. These bubbles create a jetting force that facilitates the exfoliation of MoS_2 nanosheets [123]. Although MoS_2 exfoliation was accomplished in this study, information on the size of MoS_2 nanosheets and the exfoliation yield was not provided. Then, using anode exfoliation in 0.5 M Na_2SO_4 solution, Niu et al. effectively created MoS_2 nanosheets with a wide area (lateral size of 5-50 μm range), molecular layer thickness (7% of MoS_2 tiny flakes are one-layer and more than 70% of 2-5 layers), as well as low oxidation [100].

3.1.4 Liquid-Phase Exfoliation

In the liquid-phase exfoliation process, bulk crystals are transformed into single- or multi-layer 2D structures by applying external pressures, such as shear forces or ultrasonic stress, within water or organic solvents. These solutions can produce sheets and composites with potential scalability and can be made in large numbers using industrial processes. Under ultrasonic action, the solvent molecules may cause the material layers to separate or strip into separate layers by weakening their connection [124]. At the nanoscale, ultrasound also aids in the division of these layers into tiny sheets. There are now around two methods for stripping MoS_2 in solution, and the weak van der Waals forces between its layers allow it to be broken down into multiple or single layers by acoustic process. The first approach involves physical methods such as shearing, bubbling, grinding, ultrasonic treatment, and stirring [125]. Although it is entirely physical, certain chemical components could still be involved. To stop the shed flakes from recombining, for instance, surfactants like chitosan and sodium deoxycholate might be added to the solution [126]. Sometimes bubbles are created by electrolysis, and tiny bubbles may get into the material's interface and cause it to slip off. Since various methods employ different processes, liquid exfoliation is really just a broad idea. Ion intercalation, ion exchange, and sonication-assisted exfoliation are the primary

liquid exfoliation techniques, as seen in Figure 5(d-f), and may be carefully categorized [100]. Liquid exfoliation appears relatively straightforward; All that is required to create nanosheets is to immerse the bulk materials in solvents and apply the appropriate ultrasonic treatments. However, selecting the right solvent is crucial since there are so many options available. The standard solution theory states that the polarizability and ionization of various components may be used to assess the stability of a mixed solution. Israelachvili [127] described the behavior's using Eq. (13):

$$V_{(r)} = \frac{\sqrt{3I}}{4}\frac{a^6}{r^6}\frac{(n_A^2 - n_B^2)^2}{(n_A^2 + 2n_B^2)^{3/2}} \tag{13}$$

where r is the distance between two atoms, I is their ionization potential, an is their polarizability, and $V_{(r)}$ is the dispersive interatomic potential. Refractive indices n_A and n_B are used to characterises the solute and solvent. The solution will be homogenous and evenly distributed, and there will be no solute accumulation, according to the Hamaker constant [128] A, which is comparable to Eq. (14). In order to further characterises the solution, the Flory-Huggins theory [129] developed the Flory-Huggins parameter, v, taking into account the effects of solvent to solute and solvent to solvent.

$$A = \frac{3\mathrm{l}}{16\sqrt{2}}\frac{(n_A^2 - n_B^2)^2}{(n_A^2 + 2n_B^2)^{3/2}} \tag{14}$$

As can be seen, for Eqn. (13) and (14), the V(r) and A will approach zero when n_A approaches n_B, indicating that the system's total energy will be at its lowest. Thus, the solution will be homogeneous and evenly distributed, and there won't be any solute aggregation. Considering the interaction of solute to solute and solvent to solvent, the Flory-Huggins theory [129] established the Flory-Huggins parameter, v, to characterise the solution more correctly.

$$\chi = \frac{z}{2}\frac{(2\varepsilon_{AB} - \varepsilon_{AA} - \varepsilon_{BB})}{KT} \tag{15}$$

where ε is the intensity of the intermolecular communication pairwise interaction energy and *z* is the coordination of the solvent and solute. Additionally, the letters A and B stand for solute and solvent, respectively. The solute will spread well in the solvent if $\chi < 0$, indicating significant interactions between the solute and solvent. The solute molecules will be drawn to one another and form a mass to deposit if $\chi > 0$.

The theoretical analysis allows for the selection of the best solution for various materials. There is a wide variety in the surface energy of various solvents. Therefore, a few solvents with comparable surface energies for various materials may save costs and increase the likelihood of a successful sample preparation. Naturally, the surface energy matching hypothesis mentioned above is just one component. If required, further deuterogenic hypotheses will be presented for the experimental procedure described in the next sections. Coleman et al. [130] used high-temperature solvents; nevertheless, 2-D nanomaterials are prone to agglomeration as the solvent evaporates, and high boiling point solvents with a low volatility cannot be eliminated. Zhou et al. [131] found that combining volatile solvents in an optimal ratio could create a stable, well-dispersed 2D nanosheet suspension, effectively overcoming this limitation.

3.2 Bottom-Up Method

3.2.1 Chemical Vapor Deposition (CVD)

MoS_2 and high-quality transition metal dichalcogenides may be synthesized on a large scale using chemical vapour deposition (CVD) technology, mainly for the creation of MoS_2 films [132]. It is a bottom-up method that maintains the material's shape, flaws, and crystallinity. Vapour combines with the substrate in a large-scale chemical process called CVD to create thin films. Direct vaporization is used in the CVD process, also known as the vapour-solids deposition method. It produces a superior monolayer on the substrate with fewer microscopic flakes. It is possible for precursors to initiate chemical reactions at high temperatures because of their charge and sublimation into a gaseous state. Because strong sediments accumulate on the matrix surfaces during the process of condensation, it is often used to produce single-layer composite structures and multilayered transition metal MoS_2 with great control over the number of layers. For the production of large-area monolayer MoS_2 films, S powder is employed as a Sulphur source and MoO_3 powder as a molybdenum source. Monolayer films develop uniformly and consistently; however, the consistency of the material is reduced due to faults that arise during the growing process [133]. High-quality semiconductor materials are often synthesized using the CVD process, which has a lengthy history. In a conventional CVD method of MoS_2 nanosheets, solid Mo or MoO_3 powder precursors serve as Mo sources, while solid S powder or H_2S gas may serve as S sources [134, 135]. In a low-pressure container, the vaporized S and solid MoO_3 react to create the nuclei necessary for the development of MoS_2 [134]. After that, when the carrier gas flows across the substrates, MoS_2 gradually expands and increases in size.

The chemical vapor deposition (CVD) technique presents both significant advantages and notable limitations for synthesizing MoS_2 nanosheets and other nanomaterials. CVD is advantageous for producing large-area, high-crystallinity MoS_2 layers with excellent uniformity, essential for advanced applications in electronics and optoelectronics. By maintaining precise control over variables such as temperature, pressure, and precursor flow, CVD can yield atomically thin, defect-free MoS_2 nanosheets with tailored electronic properties [136]. Additionally, the scalability of CVD facilitates industrial-scale production, allowing for consistent coverage over large substrates to meet commercial demands for cost-effective, high-volume manufacturing [137]. The flexibility of the CVD process also supports the fine-tuning of MoS_2's properties, as parameters like layer number and crystal orientation can be adjusted through the precise regulation of temperature, precursor ratios, and substrate choice [138]. However, CVD demands rigorous control of growth parameters, where slight deviations can compromise product consistency and quality. Establishing an optimal environment-requiring precise substrate treatment and the selection of metal precursors-adds complexity and elevates operational costs. The high temperatures and expensive precursors further contribute to CVD's elevated cost structure, with potential material wastage from unused precursors also posing environmental concerns [139]. As CVD scales to larger production volumes, maintaining a defect-free structure becomes increasingly challenging, as even minor inconsistencies during growth can introduce defects, thus affecting the electronic performance and reliability of the final MoS_2 nanosheets. Overall, while CVD is effective for synthesizing high-quality MoS_2 nanosheets, its cost, complexity, and defect management present challenges that continue to guide research efforts toward refining this method.

The growth of MoS_2 in the CVD process typically occurs at temperatures ranging from 700 to 1000°C and often involves the use of a metal catalyst like gold (Au). Zhang et al. [140], made modifications to the preparation, resulting in MoS_2 triangular monolayers with grain sizes up to 150 µm. Alharbi et al. [141, 142], produced the largest island-density MoS_2 film in the field by using a chemical vapour deposition technique. The various synthesis methods for synthesizing MoS_2 are shown in Figure 6.

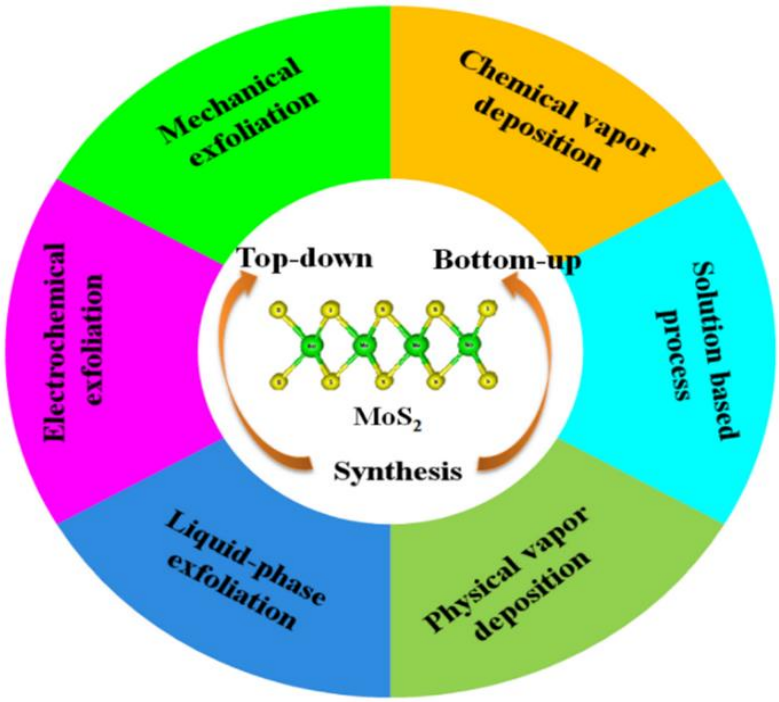

Figure 6 Different synthesis techniques for producing MoS_2 [143].

3.2.2 Hydrothermal/Solvothermal Method

MoS_2, which has a two-dimensional sheet structure, has been widely studied because of its large molybdenum and Sulphur vacancies for polarisation properties and a high specific surface area [144]. It has gained recognition as a competitive microwave absorption material due to its excellent electric conductivity, remarkable interfacial polarisation effect, and simplicity of structural design. The hydrothermal method is one of the most frequently discussed techniques for creating nanomaterials with various morphologies and thicknesses [145]. This method involves an uneven reaction with aqueous solutions of solvents or mineralizers under high pressure and low temperatures in enclosed stainless-steel vessels called autoclaves. The goal is to dissolve and recrystallize minerals that are normally quite intractable. If water is employed as a solvent, this process is referred to as hydrothermal; organic solvents are utilized in the solvothermal approach [146]. This technique may synthesize nanoparticles with high crystallinities, desirable crystalline facets, variable morphologies, and controllable sizes by varying experimental parameters like temperatures, solvent, time, etc. Hydrothermal chemical synthesis is a widely used process because it uses very little energy and, more significantly, is ecologically pleasant [147]. An example of an MoS_2 synthesis is shown in Figure 7a. Non-aqueous solvents are used as intermediates, mineralizers, and pressure carriers in the solvothermal process. It is possible to use multiple non-aqueous

solutions with different properties at the same time, producing nanomaterials with different properties. Bottom-up synthesis is used in both solvothermal and hydrothermal synthesis processes. Core-shell composites may be made using solvothermal techniques. MoS_2 nanomaterials produced using different bottom-up techniques exhibit diverse sizes, forms, morphologies, and thicknesses, making them suitable for many applications [148]. Using a hydrothermal technique and a chemical vapor deposition (CVD) approach, Yang et al. [149] achieved an RLmin of -53.03 dB at 7.86 mm.

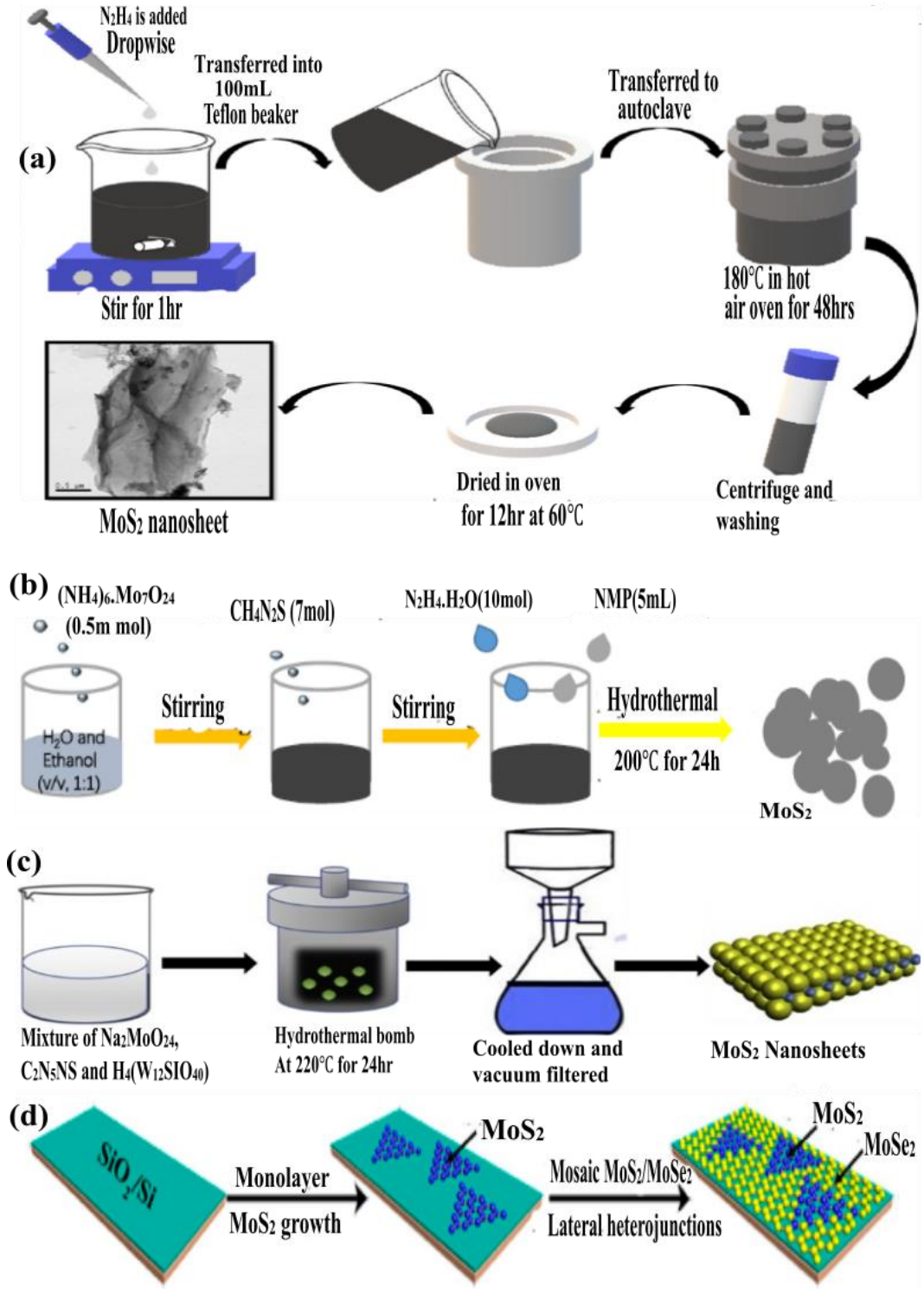

Figure 7 Schematic representation of the synthesis of MoS_2 using (a) solvothermal, (b-c) hydrothermal, and (d) CVD methods [150-152].

Ma et al. [153] produced MoS_2-PANI nanocomposites with high microwave absorption characteristics using a conventional hydrothermal method. The MoS_2-PANI nanomaterials exhibit an optimum reflection loss value of -59.79 dB at 9.68, an efficient EAB of 3.1 GHz, and a corresponding thickness of 3.44 mm within the C- and X-band frequencies. Based on their experiment, they found three things that explain why MoS_2-PANI nanocomposites are so good at absorbing microwaves: excellent electrical conductivity, smaller particle size, and improved specific surface area. Liang et al. [154] evaluated the hydrothermally produced pure MoS_2 nanosheets' microwave absorption characteristics. The results show that the significant dielectric loss produced an effective microwave reflection loss of -47.8 dB at 12.8 GHz and an efficient absorption bandwidth of 5.2 GHz. Spinel ferrites have been studied extensively in recent years because they have traditionally been used to absorb microwaves.

Using the hydrothermal technique, Liang et al. [94] created MoS_2 nanosheets with remarkable dielectric losses and microwave absorption capabilities. The resultant MoS_2 nanosheets, with their significant dielectric loss and higher interfacial polarisation, are highly desirable as an electromagnetic (EM) absorber. The findings demonstrate that MoS_2 produced at 180°C has more significant real and imaginary parts of permittivity than other samples. MoS_2 nanosheets produced at 180°C have an optimum reflection loss (RL) value of -47.8 dB at 12.8 GHz owing to their excellent electric conductivity and polarisation effect. Additionally, it has been shown that MoS_2 has an effective absorption bandwidth EAB of 5.2 GHz (<-10 dB) with absorbance thicknesses of 2.0 mm. The findings showed that, at thin thicknesses, MoS_2 nanosheets may accomplish a wide efficient absorption bandwidth EAB, making them a promising choice for microwave absorption. MoS_2 possesses adaptable semiconductor properties and a configurable band gap because electrons in the valence band are readily propelled to the conduction band by heat or electric-field activation [155]. Since activated electrons can travel like free electrons and result in substantial conduction loss, MoS_2 may be classified as a dielectric loss-type MAM. Sheet-like MoS_2 is thought to be a good candidate for absorbing microwaves because it has an extensive specific surface area and a lot of active sites that can interact with EM radiation. A schematic depiction of the synthesis of MoS_2 using hydrothermal, solvothermal, and CVD techniques is shown in Figure 7(a-d). The various synthesis methods, precursors, and applications are presented in Table 2.

Table 2 Different synthesis techniques, precursors, and their application.

Method	precursors	Synthesis condition	Properties	Application	Ref
Solvothermal method	$(NH_4)_2MoS_2$, N,N-Dimethylformamide (DMF), graphite powder and phosphorus (v) oxide.	30 mins under sonication, followed by hydrothermal processes for 10 hrs at 200°C, and finally dried by lyophilization for 10 hrs, after centrifugation, for 10 hours.	Significant surface area, minimal density, strong thermal stability, and substantial dielectric loss.	Microwave absorption	[156]
Coprecipitation method	Citric acid, ammonium hepta-molybdate tetrahydrate, and distilled water are mixed using a magnetic stirrer.	Heated for 30 m at 150°C on a hot plate with magnetic stirring, then dried and calcined between 250 and 800°C in temperature.	Continuous, rod-shaped, MoS_2-tunable nanoelectronics through a diameter of 20-150 nm	HDS and favorable tribological properties	[157]
Hydrothermal method	Deionized (DI) water containing sodium molybdate thioacetamide	Autoclaved for 24 hrs at 200°C, centrifuged for 10 minutes at 10,000 rpm, and dried for 10 hrs at 60°C.	There were about 0.64 ± 0.05 nm-long mesoporous MoS_2 crystal lattice fringes.	use of electrochemistry and supercapacitors	[158]
Solvothermal	MoS_2 powder, monoethanolamine, and zinc acetate dihydrate ($C_4H_{10}O_6Zn$)	Thermal treatment in an atmosphere of H_2/Ar	Effective absorption of 4.73 GHz microwave radiation	Attenuation and absorption of microwaves	[159]
Electrospinning technology, and hydrothermal	Magnesium acetate tetrahydrate ($C_4H_6O_4Mg{\cdot}4H_2O$), DMF, sodium molybdate ($Na_2MoO_4{\cdot}2H_2O$) and absolute alcohol	Stirred for 30 minutes and heated for 22 hours at 200°C, composites of $MgFe_2O_4/MgO/C@MoS_2$ were frozen for 8 hours at -50°C.	Significant dielectric loss, minimum density, and effective absorption bandwidth of 3.9 GHz		[160]

in situ polymerization	Sodium dodecyl benzene sulfonate (SDBS), $(NH_4)_2S_2O_8$, CN_2H_4S	pH = 1 using HCl was maintained. Autoclaved for 18 hours at 220°C, washed with deionized water and ethanol Finally, it was dried at 80°C for 12 hours.	Significant dielectric loss, minimum density, sufficient surface area and Effective absorption of 4.96 GHz microwave radiation	High-performance EM absorber	[161]
Solvothermal	$(NH_4)_6Mo_7O_{24}{\cdot}4H_2O$ and 30 mmol Thiourea	stirred for 1 h, and autoclave at 200°C for 20 h.	25% of IT-MoS_2 doped in 2H-MoS_2 nanosheet enhancing the electron carrier con.	Tuning the magnetic properties of other 2D materials.	[35]
Facile hydrothermal route	Sodium molybdite ($NaMoO_4{\cdot}2H_2O$) and Thioacetamide (CH_3CSNH_2).	the mixture was autoclaved at 200°C for 24 h and dried at 60°C	Because of its great heat resistance, the absorbent may be employed at higher temperatures.	Microwave absorption	[162]
Ball-milled method	Powdered Sulphur and molybdenum elements.	Radial ball mill with ethanol at 400 rpm for 10 hours. Tube furnaces heated to 850°C at 10°C per minute for 1 hour in a N_2 environment.	Homogeneous MoS_2 microspheres, typically measuring 1 µm. nanosheets with layer thicknesses of 19-23 nm.	fabrication of electronic devices	[163]

4. MOS_2 As MAMs

Recently, molybdenum disulfide (MoS_2), generally found as single- or few-layer nanosheets, has garnered much interest for use as electromagnetic wave absorbers [164]. The dielectric loss is largely responsible for MoS_2's unique geometrical architecture, peculiarities, and non-magnetism, which all influence its ability to absorb electromagnetic waves. Therefore, MoS_2 has enormous potential for microwave absorption. A diagram of the sample fabrication process for Fe@MoS_2 composites is shown in Figure 8. Wang et al. [165] research revealed the exceptional microwave absorption properties of exfoliated MoS_2, using Stober process. For the three-dimensional nano-flower structure composite, an optimal reflection loss (RL) coefficient of -25.0 dB to -33.0dB was discovered with a material thickness increases from 1.5 mm to 2.1 mm. The highest adequate bandwidth (RL ≤ -10) was 4.96 GHz, which covered 8.08–11.76 GHz.

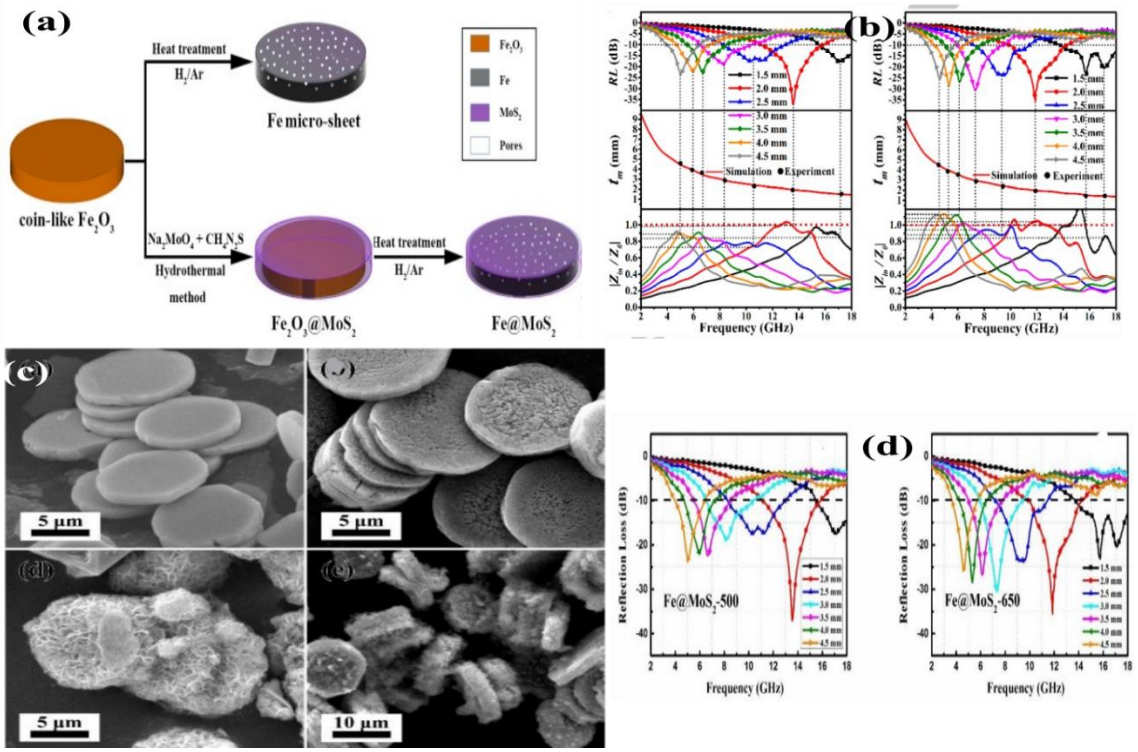

Figure 8 Schematic representation of (a) the sample synthesis procedure, (b) the quarter-wavelength matching thickness (mm), (c) microscopic SEM plates, and (d) microwave reflection loss (RL) of porous coin-like Fe and Fe@MoS_2 composites [166].

Su et al. [167] successfully synthesized MoS_2 nanospheres through the hydrothermal method. The synthesized samples exhibited a distinctive hollow, flower-like structure. The synthesized MoS_2 nanospheres had a matching thickness of 2.0 mm and a peak reflectivity loss (RL) of -45 dB at 8.3 GHz. The dielectric loss and electromagnetic wave destructive interference within the MoS_2 nanospheres are responsible for the significant broadening of the adequate absorption bandwidth observed in all samples in the X-band. In light of this, a flower-shaped MoS_2 nanosphere is a potential thin-layer, broadband, multiband, and light-weight absorber in the 8.2-12.4 GHz frequency range. Mixed-dimensional van der Waals force hybrid structures, including MoS_2, were created by Sun et al. [168]. These heterostructures included the 2-1 form (2D MoS_2/1D carbon nanotubes), the

2-3 type (2D MoS_2/3D carbon layers), and the 2-0 type (2D MoS_2/zero-D Ni nanostructures). For 0D, the optimum refraction loss (RL) is -19.7 dB at 2.92 GHz; for 1D, it is -47:9 dB at 5.60 GHz; and for 3D, it is -69:2 dB at 4.88 GHz. The MoS_2 composites have excellent microwave absorption capabilities, as can be demonstrated. Nonetheless, a little study has been done on how the spherical shape affects pure MoS_2's ability to absorb microwaves. Zhang et al. [169] developed a novel design of MoS_2/PANI-NDs composite by fusing PANI nanoneedles (PANI-NDs) with the MoS_2 nanosheet matrices through in-situ oxidative polymerization techniques. The produced composite's distinct design offered improved dielectric qualities, efficient electron transit, and adjustable electric conductivity. These beneficial characteristics produced outstanding electro-responsive results at extensively used electric field intensities. The greatest reflection loss (RL) value of -44.4 dB at 11.48 GHz for the MoS_2 nanosheets was obtained at 3 mm thickness. In mechanical automation and aerospace, a new approach to building innovative materials has been made possible by the distinctive structure of the MoS_2/PANI-NDs composite.

Zhang et al. [166] synthesized MoS_2-NS, H-MoS_2 and HH-MoS_2 nanocomposites with varied hierarchical and porous configurations using the hydrothermal technique. The absorbed microwave Interfacial polarisation and dipole orientation polarisation are used to execute the as-prepared sample polarisation, as shown in Figure 8. Additionally, the resulting composites with 30 weight percent loading have a matching bandwidth with efficient attenuation (RL < -10 dB) up to 3.32 GHz and an optimal reflection loss (RL) value of -44.67 dB at a thin thickness of 1.4 mm on the MoS_2/C display. This work offers a fresh perspective on the mechanism of MoS_2-based materials' microwave absorption and a unique understanding of new microwave absorbents with lower thicknesses, more reflection loss, and a broader absorption frequency range. Numerous initiatives have been made to improve the architectural advantages of MoS_2 absorbers, including interface design, the development of novel nanomaterials, and multilayer structural designs that optimize impedance. In general, MoS_2 is considered a popular method for enhancing the potential microwave absorption capability when combined with additional dielectric and magnetic materials. Gai et al., [170]. A simple approach for synthesizing lightweight and inexpensive materials was developed, and the latter demonstrated a narrow absorption bandwidth and poor reflection loss (RL) performance. Strong impedance matching in the composite and a variety of loss pathways, including conductive loss, dipole polarisation, and interfacial polarization, are most likely to blame for this. The greatest reflection loss (RL < -10 dB) value of -49.1 dB was obtained using a filter thickness of 2.5 mm at 6.1 GHz and a wide bandwidth of 6.4 GHz. The findings indicate that the PPy@MoS_2 composite in its current state is a promising option for high-performance, light-weight, wide-bandwidth absorbers [170].

Su et al. [171] synthesized molybdenum disulfide polypyrene (MoS_2@Ppy) nanocomposites using an in-situ polymerization technique and a microwave-assisted hydrothermal process. MoS_2's surface was evenly covered with PPy nanoparticles, and some tiny particles resembling flowers were embedded in the folds of the MoS_2. Ppy's extraordinary conductivity greatly enhanced the complicated permittivity of composites. The microwave absorbance properties of MoS_2@Ppy nanocomposite materials were thoroughly investigated. The MoS_2@Ppy nanocomposite demonstrated robust microwave energy absorption, a thin thickness, and a wide absorption bandwidth, achieving an optimum reflection loss (RL) of -61.1 dB at 11.2 GHz with a thickness of 2.28 mm. In comparison to similar materials, the MoS_2@Ppy composite outperformed comparable

materials. As very effective microwave absorbers, the MoS_2@Ppy nanocomposites offer many possible applications.

4.1 Microwave Absorption Performance of MoS_2 with MAMs

Researchers currently opt for 2D materials such as MoS_2 due to their substantial surface area, robust electrical properties, and favorable surface chemical activity [170, 171]. However, these 2D materials typically feature a single-loss process. Composite treatment with other substances has enhanced the electromagnetic wave absorption capabilities of 2 dimensional-based microwave absorbers. Magnetic metals, in particular, have drawn a lot of interest in the field of EM wave absorption because of their excellent magnetic permeability and significant magnetic loss tangent [172]. Nevertheless, metals have limited practical applications owing to their superb density and susceptibility to oxidation [10]. By combining magnetic metallic materials with 2D molybdenum sulfide (MoS_2), which offers adjustable resistivity, it becomes possible to control the permittivity and optimize the composite's overall impedance matching level. Additionally, molybdenum sulfide nanoparticles have been incorporated with other magnetic and dielectric materials to create composite fillers that interact positively with incoming radiation.

Li et al. [173], synthesized RGO/MoS_2@Fe_3O_4 nanocomposite and observed a maximum reflection loss of -49.43 at 3.0mm. According to Zhang et al., Magnetic nickel nanoparticles are embedded in MoS_2 nanosheets to create a Ni/MoS_2 nanocomposite. Their findings indicate that introducing a magnetic loss mechanism has significantly enhanced the absorption capacity of Ni/MoS_2 composites compared to pristine MoS_2. With a filler loading of 60%, the RLmin value might reach -55 dB, and the adequate absorption bandwidth (EAB) can extend to 4.0 GHz. Recent studies show that coupling magnetic materials with MoS_2 nanosheets improves microwave absorption effectiveness while raising magnetic loss [91, 174]. Fe_2O_4 nanoparticles (NPs) have become extensively employed as MAMs due to their remarkable chemical resistance and inexpensive cost. Nevertheless, they have very low microwave permeability. In contrast, magnetic metal (like Fe) NPs have higher permeability [175] but oxidize extremely fast in moist air or at high temperatures. To enhance MoS_2's absorption capabilities, core-shell Fe@Fe_2O_4 nanocomposites are a viable alternative. It is possible to prevent this oxidation by covering Fe NPs with an oxide layer. Spinel ferrite absorbers are only moderately helpful in practice because of their great density, little flexibility, singular magnetic loss, and inadequate corrosion resistance [176]. Spinel ferrites have the aforementioned limitations, so combining them with dielectric materials like graphene, MoS_2, and other conductive polymers to form magnetic/dielectric hybrids has become a typical solution [144, 177]. Lately, there has been more interest in making unique ferrites with different microstructures in this field. Zhang et al. [178] added clusters of $NiFe_2O_4$ to RGO to change the composites' electromagnetic properties as they were being made. MoS_2 cannot, however, fully match all impedances with a single dielectric loss method. This suggests that the impedance-matching capabilities of MoS_2 might be balanced with a magnetic component.

Because of their unique qualities, saturation magnetization, excellent complex permeability, and low-cost cost-conventional ferrite materials have found extensive application in the field of microwave absorption [179]. Spinel ferrites have attracted considerable interest in high-frequency devices because they have strong electromagnetic properties, effective absorption intensity, wide absorption bandwidth, thin thickness, light weight, significant magneto crystalline anisotropy, low

coercivity, high permeability, low dielectric loss, high magnetic saturation, high resistivity, high squareness ratio, and low coercivity. Consequently, they have a sizeable magnetic loss, making them potential microwave absorbers [180, 181]. The only known material that can absorb microwaves better than any other is spinel ferrite. Spinel ferrite's main benefits are its low weight and thinness, which give it a wider range of absorption and make it useful for things like stealth and space technology. On the other hand, ferrites alone have some flaws, such as low absorption, a high frame density, minimal dielectric losses, and a narrow absorption band [182].

Xing et al. [15] Used a simple hydrothermal process to create a range of MoS_2/FeS_2 composites with local heterojunctions by varying the Mo/Fe molar ratio. The MoS_2/FeS_2 heterojunction area created a compact ohmic contact and a local electric field, significantly increasing the interface polarisation loss capacity, as shown by electron holography. Thus, with a thickness of only 2 mm, an adequate absorption bandwidth of up to 6.48 GHz (from 11.52 to 18 GHz) and a maximum reflection loss value of 60.2 dB at 8.08 GHz were successfully attained. These promising results provide a path towards the logical design of 2D material-based high-performance microwave absorbers. Their distinctive structure and believable mechanisms make it possible to produce sophisticated MA materials based on 2D composites.

Liao et al. [183] synthesized the $MgFe_2O_4/MgO/C@MoS_2$ composites by hydrothermal, carbonization, and electrospinning methods. The addition of a MoS_2 layer resulted in an enhancement of the dielectric constant of the composites. These prepared composites, $MgFe_2O_4/MgO/C@MoS_2$, demonstrated a remarkable maximum RL value of -56.94 dB at 9.5 GHz with an absorber thickness of 2.7 mm and an adequate absorption bandwidth (EAB) of 3.9 GHz (8.08 to 11.98 GHz). The remarkable EM wave absorption performance of the composites may be attributed to the right impedance matching achieved by modifying the composition of the MA material, the interfacial and dipole polarisation provided by many interfaces, and the high attenuation capabilities of a 1D structure. Hence, it suggests that $MgFe_2O_4/MgO/C@MoS_2$ composites hold promise for creating lightweight and highly efficient MA materials.

Bi et al. [184] used a hydrothermal technique and the MOF self-template approach to create $CoZn/C@MoS_2@PPy$ absorbers with a 2D structure, low weight, and good performance. The primary aspects impacting the absorption performance of the $CoZn/C@MoS_2@PPy$ composites include improved impedance matching, conduction loss, and exceptional dielectric loss when MoS_2 sheets and PPy are added. The produced composites exhibit exceptional microwave absorption capabilities due to enhanced impedance matching and increased microwave attenuation. With an absorber thickness of 1.5 mm, the results showed a maximum reflection loss value of -49.18 dB at 4.56 GHz. It has been demonstrated that $CoZn/C@MoS_2@PPy$ composites might emerge as a popular choice due to their excellent microwave absorption capabilities and lightweight nature. MoS_2-based material categories for efficient microwave absorption are summarized in Figure 9. Table 3 shows the microwave absorption performance of MoS_2 with other MAMs.

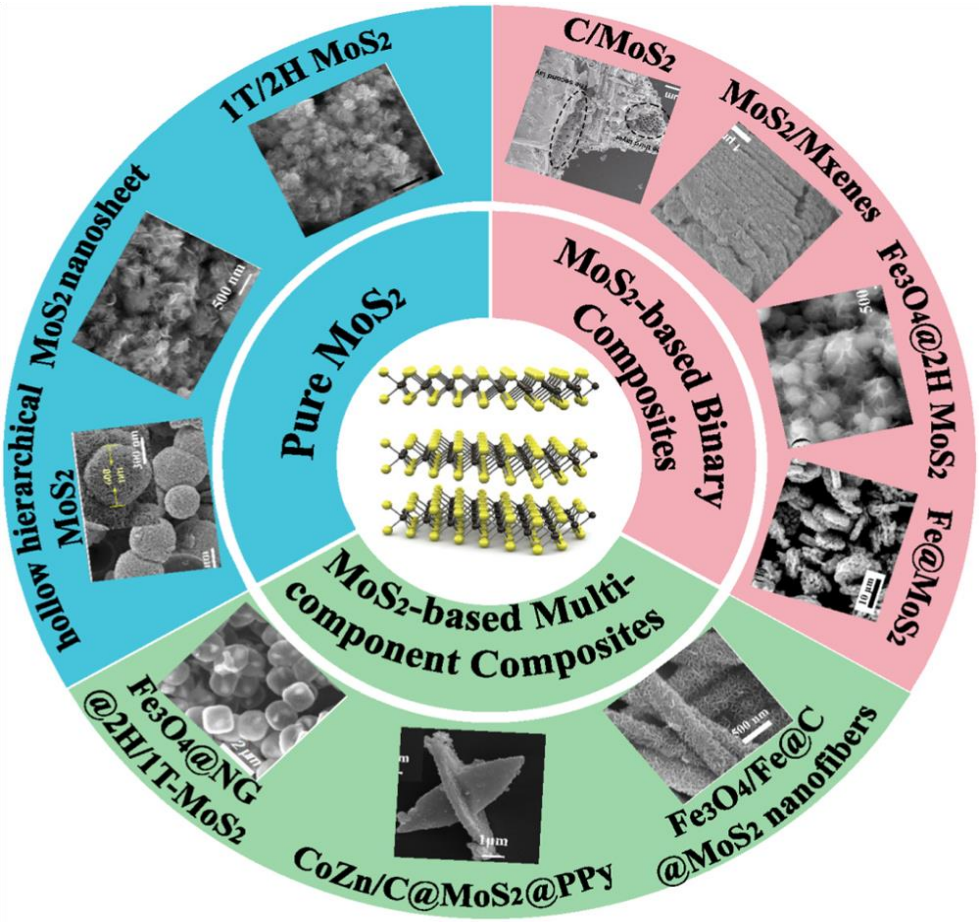

Figure 9 Summary of MoS_2-based material categories for efficient microwave absorption [185].

Table 3 Microwave Absorption Performance of MoS_2 with other MAMs.

Composite material	Method	Frequency (GHz)	*RL* (dB)	Thickness (mm)	Bandwidth (GHz)	Ref
$MgFe_2O_4/MgO/C@MoS_2$	Hydrothermal	9.5	-56.94	2.7	3.9	[184]
$BaFe_{12}O_{19}@MoS_2$	Hydrothermal	4.4	-61.0	1.7	4.9	[186]
$CoFe@MoO_2/MoS_2$	Simple hydrothermal	12.5	-54.83	2.0	6.4	[187]
Fe_3O_4@1T/2H-MoS_2	Hydrothermal	10.36	-56.22	1.8	4.7	[188]
$MoS_2/Ti_3C_2T_x$	Microwave-hydrothermal	12.2	-41.5	2.0	3.6	[189]
$CoNi_2S_4/Co_9S_8@MoS_2$	Simple hydrothermal	9.8	-50.61	2.9	8.4	[184]
MoS_2/Fe_3O_4/PANI	Facile hydrothermal	12.0	-41.05	2.2	4.4	[190]
Co_9S_8/CNTs/MoS_2	Hydrothermal	11.5	-35.4	2.5	8.4	[191]
Fe_3O_4/Fe@C@MoS_2	in-situ polymerization	11.2	-53.79	2.2	4.48	[192]
$CuFe_2O_4/MoS_2$	Solvothermal	10.4	-49.43	2.3	8.1	[193]
MoS_2/AC	Hydrothermal	10.4	-31.8	4.5	3.5	[194]
ppy@$MoS_2@Fe_3O_4$	Solvothermal	8.3	-50.65	3.8	2.0	[195]
$Co_xFe_{3-x}O_4/MoS_2$	Hydrothermal	13.5	-66.83	1.57	6.6	[70]
MoS_2/Co_3O_4	facile hydrothermal	6.9	-43.56	4.00	4.7	[196]
$ZnFe_2O_4@MoS_2$	facile hydrothermal	9.5	-61.80	3.00	5.8	[197]
CS/MoS_2-wax	Hydrothermal	12.4	-52.60	1.4	4.9	[198]
$MoS_2@Ti_3C_2T_x$	two-step hydrothermal	11.2	-51.0	4.0	4.8	[199]
RGO-MoS_2	one-pot hydrothermal	12.0	-31.57	2.5	5.9	[200]
MoS_2/RGO	Coprecipitation hydrothermal	8.72	-49.41	2.52	4.4	[201]
$CuFe_2O_4/MoS_2$	hydrothermal	10.8	-49.43	2.7	8.16	[202]
$NiS_2@MoS_2$	facile hydrothermal	12.1	-41.05	2.2	4.4	[203]

4.2 Absorption Performance of MoS_2 with Magnetic Metals Oxide

The superior magnetic loss characteristics of magnetic metallic materials, including Co, Fe, and Ni, as well as their alloys, have made them popular for microwave absorbers [204]. However, poor impedance matching makes it challenging to achieve effective microwave absorption with a single magnetic metallic material with magnetic loss [205]. When combined with magnetic metallic materials, molybdenum disulfide (MoS_2), a transversal semiconductor material with adaptive resistivity, may efficiently control the permittivity and maximize the impedance matching [156, 203]. In conclusion, magnetic materials enhance the absorption performance of MoS_2-based microwave absorbers by contributing to both magnetic loss and optimized impedance matching. The tables below present several MoS_2-based microwave absorption composites incorporating magnetic elements, varying performance among magnetic components. Specific composites achieve superior microwave absorption at reduced coating thicknesses within the same component, likely due to differences in microstructure resulting from distinct preparation procedures, which increase electromagnetic wave reflection and loss within the composite materials.

4.2.1 Absorption Performance of MoS_2 with Iron Oxide

The semiconductor characteristics of MoS_2 may be readily adjusted due to its tunable band gap. This is because heat or electric field activation can easily excite electrons in the valence band of MoS_2 to the conduction band [206]. MoS_2 may be categorized as a dielectric loss-type MAM because activated electrons can spread like free electrons and result in significant conduction loss. Specifically, MoS_2 in the form of sheets is regarded as a potential material for microwave absorption because of its enormous specific surface area, which offers a multitude of active sites that may interact with electromagnetic radiation. Research has recently shown that MoS_2 nanosheets can be hybridized with magnetic substances to improve their microwave absorption performance [172]. This results in an increase in magnetic loss and an improvement in the impedance match. Fe_3O_4 nanoparticles (NPs) have been employed as magnetically activated materials (MAMs) in many applications due to their inexpensive cost and strong chemical stability [207]. Despite this, the NPs have extremely poor microwave permeability. On the other hand, magnetic metal nanoparticles (such as Fe) have a greater permeability [208], but they oxidize readily in moist air or at high temperatures. Fe nanoparticles may be coated with an oxide layer to halt such oxidation; one example is Fe@Fe_3O_4 NPs, a promising option to improve the microwave absorption efficiency of MoS_2 NSs. Table 4 summarizes the microwave absorption performance of MoS_2 with Fe oxide. The performance of MoS_2 with iron oxide in terms of microwave absorption is shown in Table 4.

Table 4 Microwave absorption performance of MoS_2 with iron oxide.

Composites materials	**Absorption Performance**								
	Method	**Freq (GHz)**	**Max *RL* (dB)**	**Max ε**	**Max ε'**	**Max μ**	**Max μ'**	**d (mm)**	**EAB (GHz)**	**Ref**
MoS_2/Fe@Fe_3O_4	Hydrothermal	11.1	-39.4	19.40	9.60	1.33	0.13	1.90	4.2	[209]
MoS_2@Fe_3O_4@C	Hydrothermal	14.2	-51.6	12.50	3.92	1.15	0.95	2.00	6.2	[210]
MoS_2@Fe_3O_4	Hydrothermal	10.08	-48.1	16.50	7.3	1.93	0.22	2.6	4.2	[211]
MoS_2@Ppy@Fe_3O_4	Solvothermal	15.4	-32.1	6.81	2.90	1.45	0.23	2.0	4.3	[212]
MoS_2/Fe_3O_4	Solvothermal	17.5	-64.0	15.5	11.2	1.8	0.62	2.0	6.1	[213]
MoS_2/Fe@B_2O_3	Hydrothermal	14.0	-41.9	21.0	1.4	2.0	0.6	2.1	4.0	[214]
MoS_2@Fe_3O_4	Hydrothermal	10.1	-40.9	10.5	6.2	1.09	0.18	2.3	4.0	[215]
MoS_2@Fe_3O_4	Coprecipitation	14.4	-64.64	18.5	9.7	1.75	0.67	2.0	7.2	[216]
MoS_2@Fe_3O_4	Hydrothermal	13.84	-87.24	5.0	3.67	1.20	0.5	2.0	5.52	[217]
MoS_2@Fe_3O_4	Hydrothermal	8.2	-50.75	13.8	6.5	1.05	0.2	2.9	5.0	[218]
MoS_2@FeO	Hydrothermal	9.9	-37.02	10.7	1.5	1.65	0.5	2.0	4.7	[159]
MoS_2@Fe_3O_4@Pani	Hydrothermal	10.06	-40.97	10.5	1.5	1.9	0.17	2.3	4.0	[215]
Fe_3O_4/MoS_2	Hydrothermal	10.5	-55.96	14.0	7.8	1.02	0.18	2.1	4.0	[219]

4.2.2 Absorption Performance of MoS_2 with Nickel Oxide

Due to their significant impedance-matching properties and permittivity, metal oxides, ferrites, and 2D-based materials are considered excellent absorption materials. The superior morphological, structural, physiochemical, electromagnetic, and dielectric characteristics may be able to reduce losses in a higher frequency range. Creating a thin, lightweight absorber made of a highly effective material with a strong absorption capacity is necessary.

A core-shell PPy@MoS_2 heterostructure nanocomposite resembling a nanotube was synthesized by Gai et al. [220] using hydrothermal techniques and chemical oxidation polymerization. Due to its distinct heterostructures, the suggested composite exhibits significantly improved electromagnetic wave-absorbing capabilities. At 6.1 GHz, the produced PPy@MoS_2 composite demonstrated outstanding reflection loss (RL) performance with a value of -49.1 dB. The as-synthesized nanocomposite also showed a wide absorption bandwidth, which could be caused by its excellent impedance matching and variety of loss mechanisms, such as conductive loss, dipole polarisation, and interfacial polarization. Remarkably, PPy@MoS_2's broadest bandwidth of 6.4 GHz at 2.5 mm was obtained. The recently created PPy@MoS_2 may be an effective option for mitigating electromagnetic pollution due to its carefully managed preparation procedure and significantly improved performance. The microwave absorption performance of MoS_2 with nickel oxide is shown in Table 5.

Table 5 Microwave absorption performance of MoS_2 with Nickel oxide.

Composites materials	**Absorption Performance**								
	Method	**Freq (GHz)**	**Max *RL* (dB)**	**Max ε**	**Max ε'**	**Max μ**	**Max μ'**	**d (mm)**	**EAB (GHz)**	**Ref**
$NiFeO_4$@MoS_2	Hydrothermal	18.0	-45.76	10.2	2.82	1.23	0.21	1.9	5.0	[221]
$NiSO_2$@MoS_2	Hydrothermal	12.08	-41.05	14.0	0.5	-	-	2.2	4.4	[203]
Ni_3S_4@PPy@MoS_2	Hydrothermal	10.1	-51.29	14.0	2.6	-	-	2.3	3.2	[222]
MoS_2/Ni powders	Electroless plating route	9.4	-44.7	13.2	4.1	1.2	0.1	2.00	2.6	[223]
MoS_2- Ni-/wax	chemical reduction	13.8	-25.1	10.7	7.2	1.05	0.1	1.6	4.2	[224]
MoS_2/Ni	chemical reduction	6.0	-55	16.7	5.6	1.4	0.28	3.0	4.0	[225]
MoS_2/Ni	Hydrothermal	13.7	-58.08	12.6	7.4	1.12	0.12	2.0	5.19	[72]

4.2.3 Absorption Performance of MoS_2 with Cobalt Oxide

MoS_2's electrical performance may be easily regulated, and its microwave absorption characteristic is enhanced by the abundance of geometrical structures with distinctive surface and interface features, such as flake and flower-like structures, that are efficiently designed [226]. The topic of microwave absorbers has seen a surge in attention due to the discovery of composites based on MoS_2. To enhance their overall performances, Long et al. [227] created core-shell-structured $Co_{0.6}Fe_{2.4}O_4$@MoS_2NCs by designing and synthesizing them using a simple two-step hydrothermal process. The as-prepared core-shell-constructed $Co_{0.6}Fe_{2.4}O_4$@MoS_2NCs demonstrated excellent absorption, thin thickness, wide absorption bandwidth, and good stability. The maximum reflection loss of -79.9 dB at 11.2 GHz was obtained with a 2mm thickness and an adequate absorption bandwidth of 5.96 GHz.

Zhu et al. [228] used a simple hydrothermal method for fabricating a flower-like CoS_2@MoS_2 composite implanted within RGO. It is shown that the as-synthesized composites' exceptional attenuation capacity, improved impedance matching, distinctive surface shape, and microstructure are responsible for the enhanced microwave adsorption capabilities. The lowest reflection loss (RL) of -58.0 dB was achieved at 13.76 GHz with a 2.4 mm thickness. The corresponding effective absorption bandwidth reaches 6.24 GHz, from 11.76 to 18 GHz (Figure 10). Based on these findings, the as-synthesized composites appear to be desirable choices for outstanding performance and are thin, broadband, and adaptable microwave absorbers.

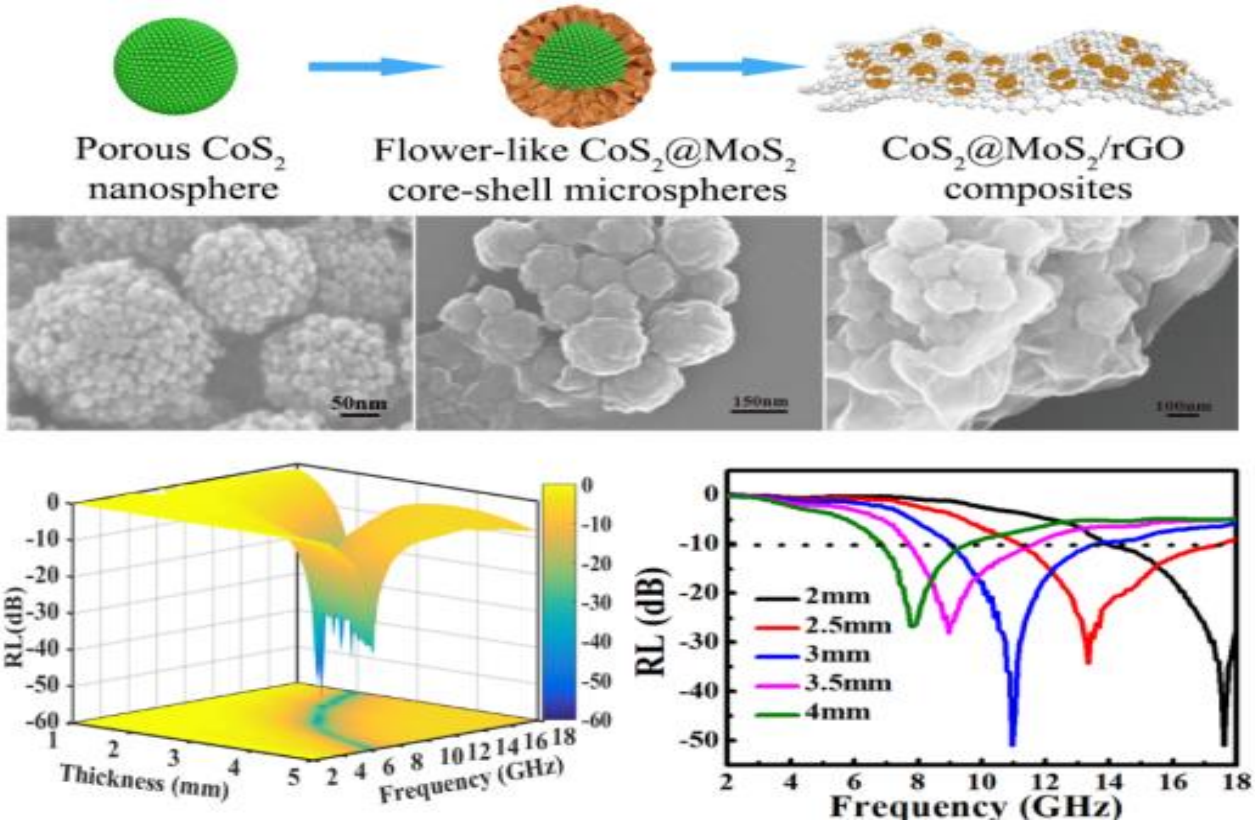

Figure 10 Microwave absorption performance of CoS_2@MoS_2 composites [228].

The microwave absorption performance of MoS_2 with cobalt oxide is shown in Table 6. Figure 9 illustrates the CoS_2@MoS_2 composites' microwave absorption capability.

Table 6 microwave absorption performance of MoS_2 with Cobalt oxide.

Composites materials		**Absorption Performance**								
	Method	**Freq (GHz)**	**Max *RL* (dB)**	**Max ε**	**Max ε'**	**Max μ**	**Max μ'**	**d (mm)**	**EAB (GHz)**	**Ref**
$CoFe_2O_4$@MoS_2	Solvothermal	13.2	-68.5	27.2	15.3	1.0	0.05	1.81	4.5	[69]
MoS_2/$CoFe_2O_4$	Hydrothermal	16.2	-55.3	14.4	9.6	1.0	0.12	1.6	6.3	[229]
MoS_2/$CoFe_2O_4$	"	12.1	-53.1	10.0	7.2	1.4	0.13	2.5	6.6	[230]
CoZn/C@MoS_2@PPy	"	15.8	-49.18	16.5	7.2	1.15	0.20	1.5	4.5	[231]
MoS_2@$CoNi_2S_4$/Co_9S_8	"	9.2	-50.61	14.0	6.4	1.03	0.23	2.9	8.4	[232]
Co/C@MoS_2	"	12.3	-63.6	26.2	14.32	1.2	0.82	2.4	7.4	[233]
CoNi@voidC@MoS_2	"	17.40	-50.90	10.2	2.82	1.23	0.21	2.7	7.0	[234]
Co/C@MoS_2	"	8.88	-52.76	15.2	4.62	1.25	0.10	2.5	3.8	[235]

4.3 Absorption Performance of MoS_2 Combined with Various Metal Oxides

Prominent 2-dimensional metallic oxides include perovskite oxide nanosheets such as $Bi_4Ti_3O_{12}$, $LaNb_2O_7$, $(Ca, Sr)_2Nb_3O_{10}$, and $CaLaNb_2TiO_{10}$, as well as titania-based nanosheets ($Ti_{0.87}O_2$). The oxide oxides above are appropriate for MAMs because they typically have exceptionallyhighly complex permittivity (usually >100). However, the literature on this subject is limited because of their great permittivity, which makes it difficult to achieve impedance matching. Their use is increasingly common in microwave dielectric materials [236, 237]. A common two-dimensional substance in transitional-metal chalcedony is MoS_2. Because of their qualities as semiconductors, exfoliated MoS_2 nanosheets are thought to be a viable option for employment in microwave absorption. Greater impedance matching with free space may be achieved more easily with these transitional-metal chalcogenides because they have a lower relative complicated permittivity and a smaller conductivity. Ning et al. [238] synthesized few-layered MoS_2 nanosheets (MoS_2-NS) using bulk MoS_2 via the top-down exfoliation approach. The EAB reached up to 4.1 GHz (9.6-13.76 GHz), while the highest reflection loss (RL) value of the prepared material is -38.42 dB. The imperfections causing significant dielectric relaxations, which are advantageous for enhancing the imaginary part of the relative permittivity (ε''), are demonstrated in the absorption mechanism. Also, MoS_2-NS has a large specific surface area, which makes it more likely for more transmission channels to form in microwave absorbers. The nanosheet nanoparticles cause conductive loss and have many conductive paths. Liang et al. [239] used a basic hydrothermal process to produce MoS_2 nanosheets of material. Their research indicates that the outermost areas of the resulting material may vary depending on the hydrothermal temperature. Compared to the other samples, it shows that the MoS_2 synthesized at 180°C has a greater permittivity and a greater surface area of 40.48 m^2/g. When MoS_2 nanosheets are 2.2 mm thick, their lowest relative sensitivity (RL) is -47.8 dB, and they have a broad frequency-dependent 4.5 cover (11-15.5 GHz).

Dai et al. [240] synthesized flower-shaped $MoS_2@Bi_2Fe_4O_9$ microspheres with a hierarchical structure as an electromagnetic wave absorber using a simple two-step hydrothermal method. With a sample thickness of 2.8 mm, the produced nanocomposite showed a maximum reflection loss value of -52.3 dB at 12.4 GHz. It also demonstrated an adequate absorption bandwidth of 5.0 GHz (10.4-15.4) with a reflection loss below -10 dB**.** The study found that MoS_2 nanosheets and $Bi_2Fe_4O_9$ MPLs work synergistically to create flower-like $MoS_2@Bi_2Fe_4O_9$ MPs that can take advantage of the advantages of both multi-interfaces created by multi-polarisation and reflection. The development of a hierarchical structure consisting of a multiferroic core and a dielectric shell shaped like a flower offers a promising avenue for the discovery of a novel ultralight electromagnetic wave absorber candidate. The $MoS_2@Bi_2Fe_4O_9$ MPs' SEM pictures, HRTEM pictures, SAED pictures, reflection loss curves, and microwave absorption processes are shown in Figure 11.

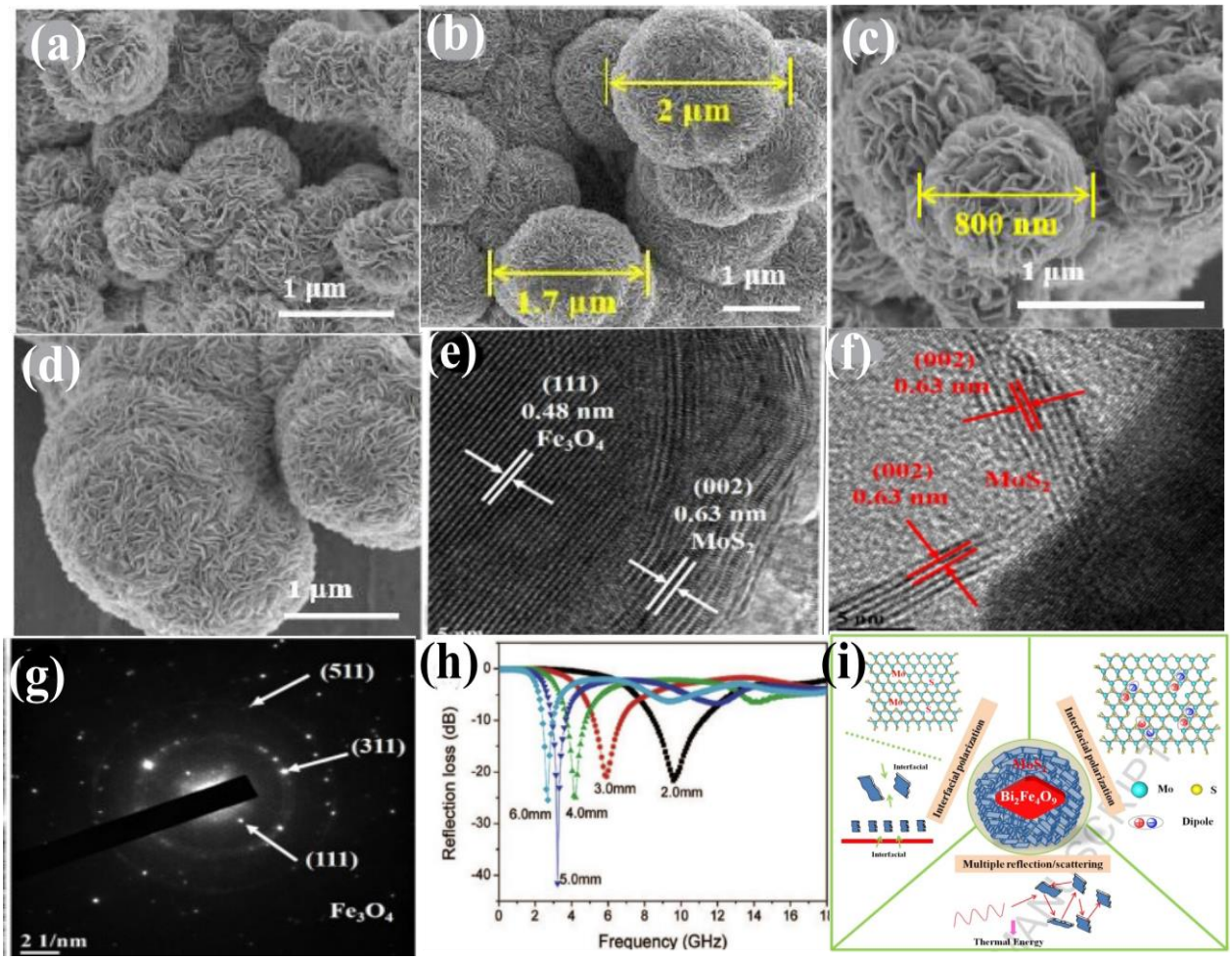

Figure 11 Illustration of SEM pictures (a-d), HRTEM photographs (e-f), SAED pictures (g), reflection loss curves (h), and microwave absorption processes (i) of MoS_2@$Bi_2Fe_4O_9$ MPs [240].

4.4 Absorption Performance of Core-Shell Structure MoS_2 Composite

Despite its widespread use in military and commercial applications, creating microwave absorbers with adjustable and highly efficient electromagnetic absorbing capability is stillchallengingoday [228]. In order to develop matrices that include microwave-absorbing materials, single solid particles such as ferrites, oxide ceramics or alloys, and metallic magnets are often used as fillers [241]. However, their practical uses are considerably limited due to their constant high density, poor stability, and large loading content. MoS_2 features a direct energy gap and a non-centrosymmetric structure. Consequently, MoS_2's outstanding electrical qualities as a semiconductor material make it a viable option for microwave absorption applications [242]. MoS_2 sheets are helpful as high-frequency absorbers because of their various advantages, which include reduced density, improved chemical durability, and special telecommunications transporting qualities [243]. Liao et al. [244] used hydrothermal processes and modified Stöber methods to effectively synthesize a core-shell Fe_3O_4@SiO_2@MoS_2 binary structure with dual shell layers. The electromagnetic characteristics of the composites were discovered to be efficiently altered when two separate layers of dielectric materials, SiO_2 and MoS_2, were wrapped around the outer layer of Fe_3O_4 nanostructures. The as-synthesized composite materials show excellent microwave

absorption performance with a maximum reflection loss value of -62.98 dB at a 5.44 GHz thickness of 1.83 mm. Additionally, its highest EAB of 5.75 GHz readily satisfies the lightweight criteria. The results indicate that the ternary core-shell composite is a viable option for high-performance microwave absorbers. Zhang et al. [82] successfully synthesized a core-shell hetero-structure MoS_2/RGO hybrid exhibiting improved microwave absorption characteristics and an extended bandwidth using a straightforward one-step hydrothermal technique. The as-synthesized composite's maximum reflection loss value of -48.41 dB was obtained at an 8.16 GHz thickness of 2.52 mm with a wide band absorption bandwidth of 4.19 GHz. The findings provide a new avenue for creating superior MA materials for real-world uses.

4.5 Applications

Under typical conditions, MoS_2-based microwave-absorbing nanomaterials are primarily employed in electronic gadgets for the following purposes:

4.5.1 For General Public Usage

These materials may be primarily integrated within electronic devices such as communication cabinets, laptop computers, and mobile phones for general consumer applications [245]. Additionally, they may be used to lessen the noise and radiation from different electronic devices [246]. Furthermore, they can mitigate internal electromagnetic interference, including resonance and leakage within barrier frames, as well as interference from low-frequency echo and low-frequency coupling conductance radiation [247]. Additionally, they might be used between the cooling modules and the semiconductor [248]. Furthermore, as the 5G era develops quickly, new technologies like artificial intelligence have significantly enhanced the quality of life. The use of microwave absorption materials, for example, precisely eliminates the pervasive electromagnetic wave pollution interference in devices like printed circuit boards, adaptable circuit boards, noncontact sensors of liquid crystal polymers, and no-crosstalk piezoelectric sensors. Furthermore, the performance of microwave-absorbing materials has critical implications in medical fields, particularly for therapeutic applications. These applications are progressively expanding across multidisciplinary domains, including electronics, life sciences, chemistry, structural engineering, medical practice, and materials science.

4.5.2 For Broad Accessibility Across Diverse User Groups and Applications

2D-MoS_2 is the most promising and appropriate material for flexible electronics because of its exceptional optoelectronic and excellent mechanical qualities, such as its outstanding stiffness and breaking stress. However, challenges such as limited thermal stability, inconsistent doping, ambient stability, and production costs remain. To achieve favorable results, flexible MoS_2 is integrated with an epoxy-based photoresist (SU-8) as an encapsulation layer and employed as a non-degenerate n-type dopant [249]. Two-dimensional MoS_2 serves as an active layer in heterojunction solar devices with substrates such as aluminum (Al), silicon (Si), and silver (Ag), making it valuable in photovoltaic applications. Studies have reported an efficiency of 5.23% [250]. Furthermore, MoS_2 has demonstrated a power conversion efficiency of 8.11% when applied directly in solar cells, attributed to its dangling bonds, chemical reactivity, and unique band structure.

With an energy conversion efficiency of 3.69%, MoS_2-based nanocomposites have recently been used as an alternative electrode in dye-sensitized solar cells (DSSCs) [251]. When combined with other materials, the MoS_2-forming hybrid phototransistor is thought to offer new optoelectronic possibilities. A phototransistor with a photovoltaic efficiency of 3.03% has been developed as a result of the hybridization of 2D materials, such as MoS_2 quantum dots and indium selenide (lnSe) nanosheets [252].

4.5.3 For Use in Defense Applications

Stealth materials, also known as microwave absorption materials, are critical components in modern military technology, contributing to weaponry and defensive systems [253]. To get the greatest immediate military advantages, stealth materials might not only boost aggressiveness but also decrease detection rates and raise their own survival rates [254]. Stealth materials are now commonly employed in explosives, missiles, naval vessels, aircraft, and various ground combat vehicles [255]. In ground-based weaponry, they play a crucial role in preventing detection by aerial radar, infrared sensors, radar-guided missiles, and laser-guided munitions [256]. Primarily, stealth technology is essential in shielding combat aircraft from detection by infrared machinery, aerial fire control radar, and aeronautical early warning aircraft radar [257].

4.6 Summery

In summary, we have thoroughly examined current developments in 2-D MoS_2-based microwave-absorbing materials and their uses. Continued investigation into the properties of microwave-absorbing materials is essential to meet the demands of increasingly complex electromagnetic environments.

We examine the following elements of research significance:

I. Further research into the novel absorbing loss process within MoS_2-based absorbent materials is essential [258]. The use of the electron holographic of visual magnetic resonance, density functional theory to compute charge distribution and conduction, and finite element analysis to assess the contribution of the macroscopic structure are some of the new methods used to further explore the loss mechanism inside the material at the micro level [259]. The material's internal and external absorption processes are examined from a micro and macro perspective, and their impact on performance is evaluated.

II. Materials derived from MoS_2 that exhibit microwave absorption must be designed with multifunctionality in mind. For instance, thermal conductivity-absorbing materials are a novel kind of multipurpose electromagnetic protection material; when electronic equipment develops quickly, thermal conductivity-absorbing indicators' performance needs rise [260]. One of the primary focus areas for future research will be the development of innovative composite materials that exhibit high thermal resistance and effective electromagnetic wave absorption capabilities. There are several possible uses for flexible and compressible microwave-absorbing materials in wearable devices to safeguard human health [261, 262]. In the future, architectural surfaces may be coated with hydrophobic microwave-absorbing materials that exhibit low thermal conductivity. This would integrate multiple functionalities, including thermal insulation, self-cleaning properties, and the mitigation of electromagnetic pollution [263, 264].

III. The foundational principle for developing microwave-absorbing materials remains 'thin, lightweight, broad-spectrum, and robust. Multiband compatibility for stealth materials is required due to the multiband nature of battlefield detection systems [265]. As a result, the material must work with a variety of frequency ranges [266]. Several MoS_2-based microwave-absorbing materials now exhibit high absorption, although broad band development is still pending [267].
IV. Numerous studies have shown that hollow fibers, hollow microspheres, core-shell structures, and porous architectures enhance absorption performance, increase multiple reflections, and reduce material density [268]. Therefore, further research into other wave-absorbing processes as well as the design and preparation of novel wave-absorbing nanomaterials with multicomponent composites, multilayered structures, and complex microstructures are potentially possible avenues for advancement.

5. Conclusions

Developing MAMs with low density, broad bandwidth, and excellent performance remains one of the most promising areas of research in order to address and overcome these difficulties and issues efficiently. Following years of rigorous study, 2D materials are now progressively playing a significant role in MAMs. Relevant efforts in the last several years have shown the superior MA characteristics of MoS_2. Because of its thin layer property and high surface area, MoS_2 offers a lot of interfaces that may be used to reduce inner scattering losses and enhance interfacial polarisation in microwave radiation. A range of regulated structures with wideband absorption capabilities, including layered stacking and core-shell siding, has been designed using the 2D MoS_2 materials as a component of the structure structure component. Furthermore. Due to their superb processability, 2D materials may be coupled with other materials to create multi-functional, multi-band electromagnetic absorbers.

MoS_2 also has a reduced permittivity due to its lesser electrical conductivity, which enables improved impedance matching to free space. MoS_2 has a few issues as well. (1) extremely high density. (2) Greater material loading is required as a result of low conductivity. (3) Conductivity has an impact on conduction losses as well. Furthermore, its conductivity affects its conduction loss. Appropriate microscopic structures and heterojunctions based on 2-dimensional MoS_2 may be constructed to solve the drawbacks. Additional advancements in the absorbers' electromagnetic attenuation and impedance matching properties are required in the search for more effective absorbers. Additional alternatives could potentially arise within the structure, linking the components simultaneously. A straightforward and sustainable synthesis preparation procedure is needed for the material preparation process. MoS_2 is a 2D compound material; further in-depth research is required to understand the absorption process. More information is required to know how the components work together to increase absorption performance, particularly in multi-component MoS_2-based composites.

In conclusion, more discussion is necessary on the correlation between the microstructure as well as the morphology of MoS_2 and its composites since this will aid in the development of modern, adaptable electronic devices. This research delivers a comprehensive evaluation of MoS_2-based microwave absorption materials (MAMs), mainly focusing on enhanced absorption properties achieved through metal oxide integration. Findings reveal that MoS_2-metal oxide composites

significantly improve microwave absorption efficiency, with in-depth insights provided into the mechanisms responsible for this optimized performance across various applications. In a nutshell, despite the many obstacles and problems present in the current generation of MoS_2-based composite absorbing materials, we think that by improving hybridization and building hierarchical structures, these absorbers may become great MAMs. Furthermore, novel structure, technology, mechanism, multifunctionality, and other factors should be the focus of future developments in microwave absorber materials.

Acknowledgments

The authors are grateful for access to the measurement facilities provided by the Institute of Nanoscience and Nanotechnology (ION2) and the Department of Physics, Faculty of Science, Universiti Putra Malaysia. Additional gratitude is extended to the Fundamental Research Grant Scheme (FRGS), Ministry of Higher Education (MOHE), Grant No. (FRGS/1/2023/STG07/UPM/02/8) for funding.

Author Contributions

Yusuf Sani: Writing – Original Draft; Raba'ah Syahidah Azis: Supervision, Writing, Review & Editing; Ismail Ismayadi: Supervision, Investigation & editing; Yaakob Yazid: Supervision, review & editing; Chen Soo Kien: Review & Editing; Mohd Mustafa Awang Kechik: Review & Editing; Lim Kean Pah: Review & Editing.

Competing Interests

The authors have declared that no competing interests exist.

References

1. Yang N, Luo ZX, Zhu GR, Chen SC, Wang XL, Wu G, et al. Ultralight three-dimensional hierarchical cobalt nanocrystals/N-doped CNTs/carbon sponge composites with a hollow skeleton toward superior microwave absorption. ACS Appl Mater Interfaces. 2019; 11: 35987-35998.
2. Wang Y, Han X, Xu P, Liu D, Cui L, Zhao H, et al. Synthesis of pomegranate-like Mo_2C@C nanospheres for highly efficient microwave absorption. Chem Eng J. 2019; 372: 312-320.
3. Wu Z, Pei K, Xing L, Yu X, You W, Che R. Enhanced microwave absorption performance from magnetic coupling of magnetic nanoparticles suspended within hierarchically tubular composite. Adv Funct Mater. 2019; 29: 1901448.
4. Zhang D, Liang S, Chai J, Liu T, Yang X, Wang H, et al. Highly effective shielding of electromagnetic waves in MoS_2 nanosheets synthesized by a hydrothermal method. J Phys Chem Solids. 2019; 134: 77-82.
5. Sani Y, Ismail I, Yaakob Y, Karim MK, Mohammed J, Alhaji BM. Ultra-wide bandwidth electromagnetic wave and enhanced microwave absorption of $Cu_{0.5}Ni_{0.5}Fe_{1.9}Mn_{0.1}O_4$@$CaTiO_3$@MWCNTs nanocomposite in X-band frequency. Diam Relat Mater. 2023; 139: 110325.
6. Cui X, Liang X, Liu W, Gu W, Ji G, Du Y. Stable microwave absorber derived from 1D customized heterogeneous structures of Fe_3N@C. Chem Eng J. 2020; 381: 122589.

7. Xu J, Sun L, Qi X, Wang Z, Fu Q, Pan C. A novel strategy to enhance the multiple interface effect using amorphous carbon packaged hydrogenated TiO_2 for stable and effective microwave absorption. J Mater Chem C. 2019; 7: 6152-6160.
8. Wu Z, Yao C, Meng Z, Deng Y, Wang Y, Liu J, et al. Biomass-derived crocodile skin-like porous carbon for high-performance microwave absorption. Adv Sustain Syst. 2022; 6: 2100454.
9. Ye X, Chen Z, Ai S, Hou B, Zhang J, Liang X, et al. Synthesis and microwave absorption properties of novel reticulation SiC/Porous melamine-derived carbon foam. J Alloys Compd. 2019; 791: 883-891.
10. Zhao Z, Xu S, Du Z, Jiang C, Huang X. Metal-organic framework-based PB@MoS_2 core-shell microcubes with high efficiency and broad bandwidth for microwave absorption performance. ACS Sustain Chem Eng. 2019; 7: 7183-7192.
11. Shen W, Ren B, Wu S, Wang W, Zhou X. Facile synthesis of RGO/$SmFe_5O_{12}$/$CoFe_2O_4$ ternary nanocomposites: Composition control for superior broadband microwave absorption performance. Appl Surf Sci. 2018; 453: 464-476.
12. Wu Z, Chang J, Guo X, Niu D, Ren A, Li P, et al. Honeycomb-like bamboo powders-derived porous carbon with low filler loading, high-performance microwave absorption. Carbon. 2023; 215: 118415.
13. ur Rehman S, Ahmed R, Ma K, Xu S, Tao T, Aslam MA, et al. Composite of strip-shaped ZIF-67 with polypyrrole: A conductive polymer-MOF electrode system for stable and high specific capacitance. Eng Sci. 2020; 13: 71-78.
14. Xiang G, Chen M, Ni Z, Shen Y, Xu L. Synthesis of a hollow-structured flower-like Fe_3O_4@MoS_2 composite and its microwave-absorption properties. RSC Adv. 2021; 11: 20180-20190.
15. Qiu J, Zhang M, Zhao R, Sun X, He D. In-situ fabrication of Ni^{2+}/Zn^{2+}-polydopamine complex derived FeCo@C/Ni@C cubic nanocages towards enhanced electromagnetic performance. Adv Compos Hybrid Mater. 2024; 7: 232.
16. Liu P, Ng VM, Yao Z, Zhou J, Lei Y, Yang Z, et al. Facile synthesis and hierarchical assembly of flowerlike NiO structures with enhanced dielectric and microwave absorption properties. ACS Appl Mater Interfaces. 2017; 9: 16404-16416.
17. Toh RJ, Sofer Z, Luxa J, Sedmidubský D, Pumera M. 3R phase of MoS_2 and WS_2 outperforms the corresponding 2H phase for hydrogen evolution. Chem Commun. 2017; 53: 3054-3057.
18. Han SA, Bhatia R, Kim SW. Synthesis, properties and potential applications of two-dimensional transition metal dichalcogenides. Nano Converg. 2015; 2: 17.
19. Manzeli S, Dumcenco D, Migliato Marega G, Kis A. Self-sensing, tunable monolayer MoS_2 nanoelectromechanical resonators. Nat Commun. 2019; 10: 4831.
20. Cao J, Zhou J, Chen J, Wang W, Zhang Y, Liu X. Effects of phase selection on gas-sensing performance of MoS_2 and WS_2 substrates. ACS Omega. 2020; 5: 28823-28830.
21. Xie A, Guo R, Wu L, Dong W. Anion-substitution interfacial engineering to construct C@MoS_2 hierarchical nanocomposites for broadband electromagnetic wave absorption. J Colloid Interface Sci. 2023; 651: 1-8.
22. Al-Ansi N, Salah A, Drmosh QA, Yang GD, Hezam A, Al-Salihy A, et al. Carbonized polymer dots for controlling construction of MoS_2 flower-like nanospheres to achieve high-performance Li/Na storage devices. Small. 2023; 19: 2304459.

23. Javed MS, Zhang X, Ali S, Shah SS, Ahmad A, Hussain I, et al. Boosting the energy storage performance of aqueous NH_4^+ symmetric supercapacitor based on the nanostructured molybdenum disulfide nanosheets. Chem Eng J. 2023; 471: 144486.
24. Ai K, Ruan C, Shen M, Lu L. MoS_2 nanosheets with widened interlayer spacing for high-efficiency removal of mercury in aquatic systems. Adv Funct Mater. 2016; 26: 5542-5549.
25. Chhowalla M, Shin HS, Eda G, Li LJ, Loh KP, Zhang H. The chemistry of two-dimensional layered transition metal dichalcogenide nanosheets. Nat Chem. 2013; 5: 263-275.
26. Siao MD, Shen WC, Chen RS, Chang ZW, Shih MC, Chiu YP, et al. Two-dimensional electronic transport and surface electron accumulation in MoS_2. Nat Chem. 2018; 9: 1442.
27. Jia D, Li X, Cai R, Ma B, Zhao Q, Chigan T, et al. Interfacial covalent bonding of Ni doped $MoS_2/TiO_2/Ti_3C_2T_x$ composites for electromagnetic wave absorption performance. Appl Surf Sci. 2023; 638: 158116.
28. Wang YQ, Ding R, Zhang YC, Liu BW, Fu Q, Zhao HB, et al. Gradient hierarchical hollow heterostructures of $Ti_3C_2T_x$@RGO@MoS_2 for efficient microwave absorption. ACS Appl Mater Interfaces. 2023; 15: 32803-32813.
29. Zhou J, Lan D, Zhang F, Cheng Y, Jia Z, Wu G, et al. Self-assembled MoS_2 cladding for corrosion resistant and frequency-modulated electromagnetic wave absorption materials from X-band to Ku-band. Small. 2023; 19: 2304932.
30. Hu W, Zhou M, Fu H. Impedance matching optimization of hierarchical carbon fiber@MoS_2@PANI nanocomposite with core-sheath structure for achieving excellent microwave absorption. Polym Adv Technol. 2023; 34: 3644-3654.
31. Krishnan U, Kaur M, Singh K, Kumar M, Kumar A. A synoptic review of MoS_2: Synthesis to applications. Superlattices Microstruct. 2019; 128: 274-297.
32. Xu H, Zhu J, Ma Q, Ma J, Bai H, Chen L, et al. Two-dimensional MoS_2: Structural properties, synthesis methods, and regulation strategies toward oxygen reduction. Micromachines. 2021; 12: 240.
33. Zeng L, Luo F, Xia X, Yang MQ, Xu L, Wang J, et al. An Sn doped 1T-2H MoS_2 few-layer structure embedded in N/P co-doped bio-carbon for high performance sodium-ion batteries. Chem Commun. 2019; 55: 3614-3617.
34. Ke Q, Zhang X, Zang W, Elshahawy AM, Hu Y, He Q, et al. Strong charge transfer at 2H-1T phase boundary of MoS_2 for superb high-performance energy storage. Small. 2019; 15: 1900131.
35. Cai L, He J, Liu Q, Yao T, Chen L, Yan W, et al. Vacancy-induced ferromagnetism of MoS_2 nanosheets. J Am Chem Soc. 2015; 137: 2622-2627.
36. ur Rehman S, Wang J, Luo Q, Sun M, Jiang L, Han Q, et al. Starfish-like C/$CoNiO_2$ heterostructure derived from ZIF-67 with tunable microwave absorption properties. Chem Eng J. 2019; 373: 122-130.
37. Xu L, Tao J, Zhang X, Yao Z, Wei B, Yang F, et al. Hollow C@MoS_2 nanospheres for microwave absorption. ACS Appl Nano Mater. 2021; 4: 11199-11209.
38. ur Rehman S, Sun M, Xu M, Liu J, Ahmed R, Aslam MA, et al. Carbonized zeolitic imidazolate framework-67/polypyrrole: A magnetic-dielectric interface for enhanced microwave absorption properties. J Colloid Interface Sci. 2020; 574: 87-96.
39. Sani Y, Ismail I, Yaakob Y, Mohammed J. Enhanced electromagnetic microwave absorbing performance of carbon nanostructures for RAMs: A review. Appl Surf Sci Adv. 2023; 18: 100455.

40. Yin X, Kong L, Zhang L, Cheng L, Travitzky N, Greil P. Electromagnetic properties of Si-C-N based ceramics and composites. Int Mater Rev. 2014; 59: 326-355.
41. Guo X, Wu Z, Chang J, Niu D, Ren A, Xu Y, et al. Boosting of electromagnetic wave absorption properties by multiple reinforcement mechanisms of metals in $FeNi_3/MoS_2$@NSAPC composites. Mater Sci Eng B. 2023; 298: 116826.
42. Wu F, Xia Y, Sun M, Xie A. Two-dimensional (2D) few-layers WS_2 nanosheets: An ideal nanomaterials with tunable electromagnetic absorption performance. Appl Phys Lett. 2018; 113: 052906.
43. ur Rehman S, Liu J, Fang Z, Wang J, Ahmed R, Wang C, et al. Heterostructured TiO_2/C/Co from ZIF-67 frameworks for microwave-absorbing nanomaterials. ACS Appl Nano Mater. 2019; 2: 4451-4461.
44. Penn SJ, Alford NM, Templeton A, Wang X, Xu M, Reece M, et al. Effect of porosity and grain size on the microwave dielectric properties of sintered alumina. J Am Ceram Soc. 1997; 80: 1885-1888.
45. Yang HJ, Cao WQ, Zhang DQ, Su TJ, Shi HL, Wang WZ, et al. NiO hierarchical nanorings on SiC: Enhancing relaxation to tune microwave absorption at elevated temperature. ACS Appl Mater Interfaces. 2015; 7: 7073-7077.
46. Liu W, Miao M, Liu JY. A novel two-dimensional material B_2S_3 and its structural implication to new carbon and boron nitride allotropes. J Mater Chem C. 2015; 3: 9921-9927.
47. Huang L, Chen C, Li Z, Zhang Y, Zhang H, Lu J, et al. Challenges and future perspectives on microwave absorption based on two-dimensional materials and structures. Nanotechnology. 2020; 31: 162001.
48. Zhang Z, Cai Z, Wang Z, Peng Y, Xia L, Ma S, et al. A review on metal-organic framework-derived porous carbon-based novel microwave absorption materials. Nanomicro Lett. 2021; 13: 56.
49. Wang K, Wan G, Wang G, He Z, Shi S, Wu L, et al. The construction of carbon-coated Fe_3O_4 yolk-shell nanocomposites based on volume shrinkage from the release of oxygen anions for wide-band electromagnetic wave absorption. J Colloid Interface Sci. 2018; 511: 307-317.
50. Zhao D, Yuan X, Li B, Jiang F, Liu Y, Zhang J, et al. Silicon carbide nanowire covered by vertically oriented graphene for enhanced electromagnetic wave absorption performance. Chem Phys. 2020; 529: 110574.
51. Xiang J, Li J, Zhang X, Ye Q, Xu J, Shen X. Magnetic carbon nanofibers containing uniformly dispersed Fe/Co/Ni nanoparticles as stable and high-performance electromagnetic wave absorbers. J Mater Chem A. 2014; 2: 16905-16914.
52. Gao N, Li WP, Wang WS, Liu DP, Cui YM, Guo L, et al. Balancing dielectric loss and magnetic loss in Fe-NiS_2/NiS/PVDF composites toward strong microwave reflection loss. ACS Appl Mater Interfaces. 2020; 12: 14416-14424.
53. ur Rehman S, Liu J, Ahmed R, Bi H. Synthesis of composite of ZnO spheres with polyaniline and their microwave absorption properties. J Saudi Chem Soc. 2019; 23: 385-391.
54. Gao S, Wang GS, Guo L, Yu SH. Tunable and ultraefficient microwave absorption properties of trace N-doped two-dimensional carbon-based nanocomposites loaded with multi-rare earth oxides. Small. 2020; 16: 1906668.
55. Zhou X, Jia Z, Feng A, Wang K, Liu X, Chen L, et al. Dependency of tunable electromagnetic wave absorption performance on morphology-controlled 3D porous carbon fabricated by biomass. Compos Commun. 2020; 21: 100404.

56. Long L, Qi X, Wang L, Cai S, Deng M. Constructing flower-like core@shell structured CoFe@MoO_2/MoS_2 magnetic nanocomposites for strong wideband microwave absorption. Mater Today Phys. 2023; 36: 101159.
57. Feng W, Liu Y, Bi Y, Su X, Lu C, Han X, et al. Recent advancement of magnetic MOF composites in microwave absorption. Synth Met. 2023; 294: 117307.
58. Mohapatra J, Joshi P, Liu JP. Low-dimensional hard magnetic materials. Prog Mater Sci. 2023; 138: 101143.
59. Dong W, Li X, Jin K, Shi Y, Wang C, Guo W, et al. Controllable synthesis of N-doped carbon nanoparticles with proper electrical conductivity for excellent microwave absorption performance. Compos Part A Appl Sci Manuf. 2023; 165: 107363.
60. ur Rehman S, Ahmed R, Liu J, Wang J, Sun M, Fang Z, et al. Decrease in the particle size and coercivity of self-assembled CoNi nanoparticles synthesized under a repulsive magnetic field. Part Part Syst Charact. 2019; 36: 1900047.
61. Li S, Xie T, Ma L, Lei Z, Huang N, Song H, et al. Ni_3Fe@N-doped carbon nanotubes 3D network induced by nanoconfined symmetry breaking for high-performance microwave absorption, corrosion protection, and pollutant purification. Carbon. 2023; 213: 118302.
62. Li Z, Liang J, Wei Z, Cao X, Shan J, Li C, et al. Lightweight foam-like nitrogen-doped carbon nanotube complex achieving highly efficient electromagnetic wave absorption. J Mater Sci Technol. 2024; 168: 114-123.
63. Liu C, Feng X, Liu S, Lin G, Bai Z, Wang L, et al. Graphene reinforced nanoarchitectonics of 3D interconnected magnetic-dielectric frameworks for high-efficient and anti-corrosive microwave absorbers. J Mater Sci Technol. 2024; 168: 194-207.
64. Xu H, He Z, Li Y, Wang Y, Zhang Z, Dai X, et al. Porous magnetic carbon spheres with adjustable magnetic-composition and synergistic effect for lightweight microwave absorption. Carbon. 2023; 213: 118290.
65. Wei H, Zhang Z, Hussain G, Zhou L, Li Q, Ostrikov KK. Techniques to enhance magnetic permeability in microwave absorbing materials. Appl Mater Today. 2020; 19: 100596.
66. Zhang Y, Si H, Liu S, Jiang Z, Zhang J, Gong C. Facile synthesis of BN/Ni nanocomposites for effective regulation of microwave absorption performance. J Alloys Compd. 2021; 850: 156680.
67. Huang C, Jin Y, Wang W, Tang L, Song C, Xiu F. Manganese and chromium doping in atomically thin MoS_2. J Semicond. 2017; 38: 033004.
68. Zhang H, Shi C, Jia Z, Liu X, Xu B, Zhang D, et al. FeNi nanoparticles embedded reduced graphene/nitrogen-doped carbon composites towards the ultra-wideband electromagnetic wave absorption. J Colloid Interface Sci. 2021; 584: 382-394.
69. Wang X, Zhu T, Chang S, Lu Y, Mi W, Wang W. 3D nest-like architecture of core-shell $CoFe_2O_4$@1T/2H-MoS_2 composites with tunable microwave absorption performance. ACS Appl Mater Interfaces. 2020; 12: 11252-11264.
70. Long L, Yang E, Qi X, Xie R, Bai ZC, Qin S, et al. Positive and reverse core/shell structure $Co_xFe_{3-x}O_4$/MoS_2 and MoS_2/$Co_xFe_{3-x}O_4$ nanocomposites: Selective production and outstanding electromagnetic absorption comprehensive performance. ACS Sustain Chem Eng. 2019; 8: 613-623.
71. Bouarissa A, Gueddim A, Bouarissa N, Maghraoui-Meherzi H. Optical response and magnetic moment of MoS_2 material. Optik. 2020; 208: 164080.

72. Wang J, Lin X, Chu Z, Huang Z, Guo T, Yang L, et al. Magnetic MoS_2: A promising microwave absorption material with both dielectric loss and magnetic loss properties. Nanotechnology. 2020; 31: 135602.
73. Cheng YC, Zhu ZY, Mi WB, Guo ZB, Schwingenschlögl U. Prediction of two-dimensional diluted magnetic semiconductors: Doped monolayer MoS_2 systems. Phys Rev B Condens Matter Mater Phys. 2013; 87: 100401.
74. Yue Q, Chang S, Qin S, Li J. Functionalization of monolayer MoS_2 by substitutional doping: A first-principles study. Phys Lett A. 2013; 377: 1362-1367.
75. Han P, Wu C, Tai J, Zhang H, Zhao G, Chen Q, et al. Improved microwave absorption properties of ferrite-RGO composites by covalent bond. J Alloys Compd. 2023; 966: 171581.
76. Wang D, Jin J, Guo Y, Liu H, Guo Z, Liu C, et al. Lightweight waterproof magnetic carbon foam for multifunctional electromagnetic wave absorbing material. Carbon. 2023; 202: 464-474.
77. Zhang D, Chai J, Cheng J, Jia Y, Yang X, Wang H, et al. Highly efficient microwave absorption properties and broadened absorption bandwidth of MoS_2-iron oxide hybrids and MoS_2-based reduced graphene oxide hybrids with hetero-structures. Appl Surf Sci. 2018; 462: 872-882.
78. Deng S, Jiang J, Wu D, He Q, Wang Y. Three-dimensional conductive network constructed by in-situ preparation of sea urchin-like $NiFe_2O_4$ in expanded graphite for efficient microwave absorption. J Colloid Interface Sci. 2023; 650: 710-718.
79. Yin Z, Wu J, Liang L, Kong C, Pervikov A, Shi H, et al. Microwave-absorbing performance of FeCoNi magnetic nanopowders synthesized by electrical explosion of wires. J Alloys Compd. 2023; 966: 171594.
80. Meng L, Li J, Li X, Wang Z, Zhou W. Fabrication of core-shell Co@HCN@PANI composite material with enhanced electromagnetic wave absorption. J Alloys Compd. 2023; 966: 171528.
81. Ban Q, Li L, Li Y, Liu H, Zheng Y, Qin Y, et al. Polymer self-assembly guided heterogeneous structure engineering towards high-performance low-frequency electromagnetic wave absorption. J Colloid Interface Sci. 2023; 650: 1434-1445.
82. Yao C, Wu Z, Liu J, Guo X, Zhang W, Huang W, et al. Construction of lychee-like MoS_2 microspheres on rice husk-derived porous carbon for enhanced dielectric loss and efficient electromagnetic wave absorption. J Mater Sci Mater Electron. 2023; 34: 1213.
83. Huang X, Liu X, Jia Z, Wang B, Wu X, Wu G. Synthesis of 3D cerium oxide/porous carbon for enhanced electromagnetic wave absorption performance. Adv Compos Hybrid Mater. 2021; 4: 1398-1412.
84. Sun X, Yuan X, Li X, Li L, Song Q, Lv X, et al. Hollow cube-like CuS derived from Cu_2O crystals for the highly efficient elimination of electromagnetic pollution. New J Chem. 2018; 42: 6735-6741.
85. Liu Z, Cui Y, Li Q, Zhang Q, Zhang B. Fabrication of folded MXene/MoS_2 composite microspheres with optimal composition and their microwave absorbing properties. J Colloid Interface Sci. 2022; 607: 633-644.
86. Ning M, Jiang P, Ding W, Zhu X, Tan G, Man Q, et al. Phase manipulating toward molybdenum disulfide for optimizing electromagnetic wave absorbing in gigahertz. Adv Funct Mater. 2021; 31: 2011229.
87. Li J, Zhou D, Wang PJ, Du C, Liu WF, Su JZ, et al. Recent progress in two-dimensional materials for microwave absorption applications. Chem Eng J. 2021; 425: 131558.

88. Uddin W, ur Rehman S, Aslam MA, ur Rehman S, Wu M, Zhu M. Enhanced microwave absorption from the magnetic-dielectric interface: A hybrid RGO@ Ni-doped-MoS_2. Mater Res Bull. 2020; 130: 110943.
89. Zhai N, Luo J, Shu P, Mei J, Li X, Yan W. 1D/2D $CoTe_2$@MoS_2 composites constructed by $CoTe_2$ nanorods and MoS_2 nanosheets for efficient electromagnetic wave absorption. Nano Res. 2023; 16: 10698-10706.
90. Luo J, Feng M, Dai Z, Jiang C, Yao W, Zhai N. MoS_2 wrapped MOF-derived N-doped carbon nanocomposite with wideband electromagnetic wave absorption. Nano Res. 2022; 15: 5781-5789.
91. Li W, Hassan A, Zedan AS, Idris M, Fayed M, Mehrez S, et al. Structural engineering of double shells decoration for preparing a high-efficiency electromagnetic wave absorber. Ceram Int. 2023; 49: 14538-14550.
92. Zhang J, Zhao M, Zhao Y, Wang J, Wu Y, Li K, et al. Microwave-assisted hydrothermal synthesis of Fe-doped 1T/2H-MoS_2 few-layer nanosheets for efficient electromagnetic wave absorbing. J Alloys Compd. 2023; 947: 169544.
93. Zhang H, Zhao Y, Zuo X, Huang H, Sun C, Fan Z, et al. Construction of chiral-magnetic-dielectric trinity composites for efficient microwave absorption with low filling ratio and thin thickness. Chem Eng J. 2023; 467: 143414.
94. Ruiz KH, Mustafa T, Yan P, Ding Q, Qiu P, Luo W, et al. Highly ordered mesoporous 1T'$MoTe_2$/m-SiO_2 composite as efficient microwave absorber. Microporous Mesoporous Mater. 2022; 336: 111894.
95. Zhang S, Liu X, Liu C, Luo S, Wang L, Cai T, et al. MoS_2 quantum dot growth induced by S vacancies in a $ZnIn_2S_4$ monolayer: Atomic-level heterostructure for photocatalytic hydrogen production. ACS Nano. 2018; 12: 751-758.
96. Sun K, Liu M, Pei J, Li D, Ding C, Wu K, et al. Incorporating transition-metal phosphides into metal-organic frameworks for enhanced photocatalysis. Angew Chem. 2020; 132: 22937-22943.
97. Liu C, Wang L, Tang Y, Luo S, Liu Y, Zhang S, et al. Vertical single or few-layer MoS_2 nanosheets rooting into TiO_2 nanofibers for highly efficient photocatalytic hydrogen evolution. Appl Catal B. 2015; 164: 1-9.
98. Ottaviano L, Palleschi S, Perrozzi F, D'Olimpio G, Priante F, Donarelli M, et al. Mechanical exfoliation and layer number identification of MoS_2 revisited. 2d Mater. 2017; 4: 045013.
99. Zhang H. Ultrathin two-dimensional nanomaterials. ACS Nano. 2015; 9: 9451-9469.
100. Liu N, Kim P, Kim JH, Ye JH, Kim S, Lee CJ. Large-area atomically thin MoS_2 nanosheets prepared using electrochemical exfoliation. ACS Nano. 2014; 8: 6902-6910.
101. Zhang P, Yang S, Pineda-Gómez R, Ibarlucea B, Ma J, Lohe MR, et al. Electrochemically exfoliated high-quality 2H-MoS_2 for multiflake thin film flexible biosensors. Small. 2019; 15: 1901265.
102. Zhang W, Zhang P, Su Z, Wei G. Synthesis and sensor applications of MoS_2-based nanocomposites. Nanoscale. 2015; 7: 18364-18378.
103. Nicolosi V, Chhowalla M, Kanatzidis MG, Strano MS, Coleman JN. Liquid exfoliation of layered materials. Science. 2013; 340: 1226419.
104. Cheng P, Sun K, Hu YH. Memristive behavior and ideal memristor of 1T phase MoS_2 nanosheets. Nano Lett. 2016; 16: 572-576.
105. Liu H, Li Y, Xiang M, Zeng H, Shao X. Single-layered MoS_2 directly grown on rutile TiO_2 (110) for enhanced interfacial charge transfer. ACS Nano. 2019; 13: 6083-6089.

106. Wang QH, Kalantar-Zadeh K, Kis A, Coleman JN, Strano MS. Transition metal dichalcogenides. Nat Publ Gr. 2012; 7: 699-712.
107. Li Z, Meng X, Zhang Z. Recent development on MoS_2-based photocatalysis: A review. J Photochem Photobiol C Photochem Rev. 2018; 35: 39-55.
108. Jeon J, Lee J, Yoo G, Park JH, Yeom GY, Jang YH, et al. Size-tunable synthesis of monolayer MoS_2 nanoparticles and their applications in non-volatile memory devices. Nanoscale. 2016; 8: 16995-17003.
109. Velicky M, Donnelly GE, Hendren WR, McFarland S, Scullion D, DeBenedetti WJ, et al. Mechanism of gold-assisted exfoliation of centimeter-sized transition-metal dichalcogenide monolayers. ACS Nano. 2018; 12: 10463-10472.
110. Desai SB, Madhvapathy SR, Amani M, Kiriya D, Hettick M, Tosun M, et al. Gold-mediated exfoliation of ultralarge optoelectronically-perfect monolayers. Adv Mater. 2016; 28: 4053-4058.
111. Shah SA, Xu L, Sayyar R, Bian T, Liu Z, Yuan A, et al. Growth of MoS_2 nanosheets on M@N-doped carbon particles (M = Co, Fe or CoFe Alloy) as an efficient electrocatalyst toward hydrogen evolution reaction. Chem Eng J. 2022; 428: 132126.
112. Frindt RF. Single crystals of MoS_2 several molecular layers thick. J Appl Phys. 1966; 37: 1928-1929.
113. Li H, Wu J, Yin Z, Zhang H. Preparation and applications of mechanically exfoliated single-layer and multilayer MoS_2 and WSe_2 nanosheets. Acc Chem Res. 2014; 47: 1067-1075.
114. Liu Y, Li R. Study on ultrasound-assisted liquid-phase exfoliation for preparing graphene-like molybdenum disulfide nanosheets. Ultrason Sonochem. 2020; 63: 104923.
115. Li Y, Kuang G, Jiao Z, Yao L, Duan R. Recent progress on the mechanical exfoliation of 2D transition metal dichalcogenides. Mater Res Express. 2022; 9: 122001.
116. Radisavljevic B, Radenovic A, Brivio J, Giacometti V, Kis A. Single-layer MoS_2 transistors. Nat Nanotechnol. 2011; 6: 147-150.
117. Novoselov KS, Jiang D, Schedin F, Booth TJ, Khotkevich VV, Morozov SV, et al. Two-dimensional atomic crystals. Proc Natl Acad Sci. 2005; 102: 10451-10453.
118. García-Dalí S, Paredes JI, Munuera JM, Villar-Rodil S, Adawy A, Martinez-Alonso A, et al. Aqueous cathodic exfoliation strategy toward solution-processable and phase-preserved MoS_2 nanosheets for energy storage and catalytic applications. ACS Appl Mater Interfaces. 2019; 11: 36991-37003.
119. Li L, Zhang D, Gao Y, Deng J, Gou Y, Fang J. Electric field driven exfoliation of MoS_2. J Alloys Compd. 2021; 862: 158551.
120. You X, Liu N, Lee CJ, Pak JJ. An electrochemical route to MoS_2 nanosheets for device applications. Mater Lett. 2014; 121: 31-35.
121. Wu W, Zhang C, Zhou L, Hou S, Zhang L. High throughput synthesis of defect-rich MoS_2 nanosheets via facile electrochemical exfoliation for fast high-performance lithium storage. J Colloid Interface Sci. 2019; 542: 263-268.
122. Sandusky RJ. Bringing design to software. J Am Soc Inf Sci. 1997; 48: 1149-1150.
123. Zhao M, Casiraghi C, Parvez K. Electrochemical exfoliation of 2D materials beyond graphene. Chem Soc Rev. 2024; 53: 3036-3064.
124. Zhang Y, Zhang R, Guo Y, Li Y, Li K. A review on MoS_2 structure, preparation, energy storage applications and challenges. J Alloys Compd. 2024; 998: 174916.

125. Gupta A, Arunachalam V, Vasudevan S. Liquid-phase exfoliation of MoS_2 nanosheets: The critical role of trace water. J Phys Chem Lett. 2016; 7: 4884-4890.
126. Zhang M, Howe RC, Woodward RI, Kelleher EJ, Torrisi F, Hu G, et al. Solution processed MoS_2-PVA composite for sub-bandgap mode-locking of a wideband tunable ultrafast Er: Fiber laser. Nano Res. 2015; 8: 1522-1534.
127. Israelachvili JN. Intermolecular and surface forces. 3rd ed. Cambridge, MA: Academic Press; 2011.
128. Coleman JN. Liquid-phase exfoliation of nanotubes and graphene. Adv Funct Mater. 2009; 19: 3680-3695.
129. Rubinstein M, Colby RH. Polymer physics. Oxford, UK: Oxford University Press; 2003.
130. Coleman JN, Lotya M, O'Neill A, Bergin SD, King PJ, Khan U, et al. Two-dimensional nanosheets produced by liquid exfoliation of layered materials. Science. 2011; 331: 568-571.
131. Zhou KG, Mao NN, Wang HX, Peng Y, Zhang HL. A mixed-solvent strategy for efficient exfoliation of inorganic graphene analogues. Angew Chem Int Ed. 2011; 46: 10839-10842.
132. Ni X, Hui C, Su N, Jiang W, Liu F. Monte Carlo simulations of electrical percolation in multicomponent thin films with nanofillers. Nanotechnology. 2018; 29: 075401.
133. Amani M, Burke RA, Ji X, Zhao P, Lien DH, Taheri P, et al. High luminescence efficiency in MoS_2 grown by chemical vapor deposition. ACS Nano. 2016; 10: 6535-6541.
134. Lin YC, Zhang W, Huang JK, Liu KK, Lee YH, Liang CT, et al. Wafer-scale MoS_2 thin layers prepared by MoO_3 sulfurization. Nanoscale. 2012; 4: 6637-6641.
135. Zhan Y, Liu Z, Najmaei S, Ajayan PM, Lou J. Large area vapor phase growth and characterization of MoS_2 atomic layers on SiO_2 substrate. Nanomicro Lett. 2012; 8: 966-971.
136. Mathew S, Reiprich J, Narasimha S, Abedin S, Kurtash V, Thiele S, et al. Three-dimensional MoS_2 nanosheet structures: CVD synthesis, characterization, and electrical properties. Crystals. 2023; 13: 448.
137. Kumar VK, Dhar S, Choudhury TH, Shivashankar SA, Raghavan S. A predictive approach to CVD of crystalline layers of TMDs: The case of MoS_2. Nanoscale. 2015; 7: 7802-7810.
138. Nawz T, Safdar A, Hussain M, Sung Lee D, Siyar M. Graphene to advanced MoS_2: A review of structure, synthesis, and optoelectronic device application. Crystals. 2020; 10: 902.
139. Liu HF, Wong SL, Chi DZ. CVD growth of MoS_2-based two-dimensional materials. Chem Vap Depos. 2015; 21: 241-259.
140. Zhang X, Nan H, Xiao S, Wan X, Ni Z, Gu X, et al. Shape-uniform, high-quality monolayered MoS_2 crystals for gate-tunable photoluminescence. ACS Appl Mater Interfaces. 2017; 9: 42121-42130.
141. Alharbi A, Armstrong D, Alharbi S, Shahrjerdi D. Physically unclonable cryptographic primitives by chemical vapor deposition of layered MoS_2. ACS Nano. 2017; 11: 12772-12779.
142. Koyappayil A, Yagati AK, Lee MH. Recent trends in metal nanoparticles decorated 2D materials for electrochemical biomarker detection. Biosensors. 2023; 13: 91.
143. Xu ZH, Tang L, Zhang SW, Li JZ, Liu BL, Zhao SC, et al. 2D MoS_2/CuPc heterojunction based highly sensitive photodetectors through ultrafast charge transfer. Mater Today Phys. 2020; 15: 100273.
144. Ren F, Guo Z, Shi Y, Jia L, Qing Y, Ren P, et al. Lightweight and highly efficient electromagnetic wave-absorbing of 3D CNTs/GNS@$CoFe_2O_4$ ternary composite aerogels. J Alloys Compd. 2018; 768: 6-14.

145. Shanmugaratnam S, Yogenthiran E, Koodali R, Ravirajan P, Velauthapillai D, Shivatharsiny Y. Recent progress and approaches on transition metal chalcogenides for hydrogen production. Energies. 2021; 14: 8265.
146. Makwana NM, Tighe CJ, Gruar RI, McMillan PF, Darr JA. Pilot plant scale continuous hydrothermal synthesis of nano-titania; effect of size on photocatalytic activity. Mater Sci Semicond Process. 2016; 42: 131-137.
147. Pokrovski GS, Roux J, Hazemann JL, Borisova AY, Gonchar AA, Lemeshko MP. In situ X-ray absorption spectroscopy measurement of vapour-brine fractionation of antimony at hydrothermal conditions. Mineral Mag. 2008; 72: 667-681.
148. Li J, Yang X, Liu Y, Huang B, Wu R, Zhang Z, et al. General synthesis of two-dimensional van der Waals heterostructure arrays. Nature. 2020; 579: 368-374.
149. Yang E, Qi X, Xie R, Bai Z, Jiang Y, Qin S, et al. Novel "203" type of heterostructured MoS_2-Fe_3O_4-C ternary nanohybrid: Synthesis, and enhanced microwave absorption properties. Appl Surf Sci. 2018; 442: 622-629.
150. Chaudhary N, Khanuja M, Islam SS. Hydrothermal synthesis of MoS_2 nanosheets for multiple wavelength optical sensing applications. Sens Actuators A Phys. 2018; 277: 190-198.
151. Hou K, Liu S, Liao G, Qiao H, Li J, Qi X. Simple hydrothermal synthesis of molybdenum disulfide and its application for a large-area photodetector. Cryst Res Technol. 2020; 55: 2000053.
152. Qi H, Wang L, Sun J, Long Y, Hu P, Liu F, et al. Production methods of van der Waals heterostructures based on transition metal dichalcogenides. Crystals. 2018; 8: 35.
153. Ma J, Ren H, Liu Z, Zhou J, Wang Y, Hu B, et al. Embedded MoS_2-PANI nanocomposites with advanced microwave absorption performance. Compos Sci Technol. 2020; 198: 108239.
154. Chen Q, Li L, Wang Z, Ge Y, Zhou C, Yi J. Synthesis and enhanced microwave absorption performance of CIP@SiO_2@$Mn_{0.6}Zn_{0.4}Fe_2O_4$ ferrite composites. J Alloys Compd. 2019; 779: 720-727.
155. Singh AK, Kumar P, Late DJ, Kumar A, Patel S, Singh J. 2D layered transition metal dichalcogenides (MoS_2): Synthesis, applications and theoretical aspects. Appl Mater Today. 2018; 13: 242-270.
156. Wang X, Zhang W, Ji X, Zhang B, Yu M, Zhang W, et al. 2D MoS_2/graphene composites with excellent full Ku band microwave absorption. RSC Adv. 2016; 6: 106187-106193.
157. Vattikuti SP, Byon C, Reddy CV, Shim J, Venkatesh B. Co-precipitation synthesis and characterization of faceted MoS_2 nanorods with controllable morphologies. Appl Phys A. 2015; 119: 813-823.
158. Ramadoss A, Kim T, Kim GS, Kim SJ. Enhanced activity of a hydrothermally synthesized mesoporous MoS_2 nanostructure for high performance supercapacitor applications. New J Chem. 2014; 38: 2379-2385.
159. Pan J, Sun X, Wang T, Zhu Z, He Y, Xia W, et al. Porous coin-like Fe@MoS_2 composite with optimized impedance matching for efficient microwave absorption. Appl Surf Sci. 2018; 457: 271-279.
160. Wang C, Li L, Li J, Wang Q, Cao J, Li J. Microwave Absorption Performance of One-dimensional Mixed Metal Oxide Nanocomposite. J Mater Sci Technol Res. 2023; 10: 117-123.
161. An D, Bai L, Cheng S, Zhang Z, Duan X, Sun Z, et al. Synthesis and electromagnetic wave absorption properties of three-dimensional nano-flower structure of MoS_2/polyaniline nanocomposites. J Mater Sci Mater Electron. 2019; 30: 13948-13956.

162. Wang H, Jin P. The electromagnetic and microwave absorbing properties of MoS_2/carbonyl iron@SiO_2. Mater Res Express. 2018; 5: 116301.
163. Balendhran S, Ou JZ, Bhaskaran M, Sriram S, Ippolito S, Vasic Z, et al. Atomically thin layers of MoS_2 via a two step thermal evaporation-exfoliation method. Nanoscale. 2012; 4: 461-466.
164. Xie A, Sun M, Zhang K, Jiang W, Wu F, He M. In situ growth of MoS_2 nanosheets on reduced graphene oxide (RGO) surfaces: Interfacial enhancement of absorbing performance against electromagnetic pollution. Phys Chem Chem Phys. 2016; 18: 24931-24936.
165. Wang H, Zhu D, Zhou W, Luo F. Electromagnetic property of SiO2-coated carbonyl iron/polyimide composites as heat resistant microwave absorbing materials. J Magn Magn Mater. 2015; 375: 111-116.
166. Zhang W, Zhang X, Wu H, Yan H, Qi S. Impact of morphology and dielectric property on the microwave absorbing performance of MoS_2-based materials. J Alloys Compd. 2018; 751: 34-42.
167. Su X, Ning J, Jia Y, Liu Y. Flower-like MoS_2 nanospheres: A promising material with good microwave absorption property in the frequency range of 8.2-12.4 GHz. Nano. 2018; 13: 1850084.
168. Sun Y, Zhong W, Wang Y, Xu X, Wang T, Wu L, et al. MoS_2-based mixed-dimensional van der Waals heterostructures: A new platform for excellent and controllable microwave-absorption performance. ACS Appl Mater Interfaces. 2017; 9: 34243-34255.
169. Zhang WL, Jiang D, Wang X, Hao BN, Liu YD, Liu J. Growth of polyaniline nanoneedles on MoS_2 nanosheets, tunable electroresponse, and electromagnetic wave attenuation analysis. J Phys Chem C. 2017; 121: 4989-4998.
170. Dutta T, Yadav N, Wu Y, Cheng GJ, Liang X, Ramakrishna S, et al. Electronic properties of 2D materials and their junctions. Nano Mater Sci. 2024; 6: 1-23.
171. Su Q, Wang B, Mu C, Zhai K, Nie A, Xiang J, et al. Polypyrrole coated 3D flower MoS_2 composites with tunable impedance for excellent microwave absorption performance. J Alloys Compd. 2021; 888: 161487.
172. Wang B, Wu Q, Fu Y, Liu T. A review on carbon/magnetic metal composites for microwave absorption. J Mater Sci Technol. 2021; 86: 91-109.
173. Li M, Cao X, Zheng S, Qi S. Ternary composites RGO/MoS_2@Fe_3O_4: Synthesis and enhanced electromagnetic wave absorbing performance. J Mater Sci Mater Electron. 2017; 28: 16802-16812.
174. Xiang Z, Song Y, Xiong J, Pan Z, Wang X, Liu L, et al. Enhanced electromagnetic wave absorption of nanoporous Fe_3O_4@carbon composites derived from metal-organic frameworks. Carbon. 2019; 142: 20-31.
175. Qi X, Deng Y, Zhong W, Yang Y, Qin C, Au C, et al. Controllable and large-scale synthesis of carbon nanofibers, bamboo-like nanotubes, and chains of nanospheres over Fe/SnO_2 and their microwave-absorption properties. J Phys Chem C. 2010; 114: 808-814.
176. Wu X, Ding Z, Song N, Li L, Wang W. Effect of the rare-earth substitution on the structural, magnetic and adsorption properties in cobalt ferrite nanoparticles. Ceram Int. 2016; 42: 4246-4255.
177. Li L, Liu S, Lu L. Synthesis and significantly enhanced microwave absorption properties of cobalt ferrite hollow microspheres with protrusions/polythiophene composites. J Alloys Compd. 2017; 722: 158-165.

178. Zhang Y, Wang X, Cao M. Confinedly implanted $NiFe_2O_4$-RGO: Cluster tailoring and highly tunable electromagnetic properties for selective-frequency microwave absorption. Nano Res. 2018; 11: 1426-1436.
179. Li J, Zhou D. Enhanced microwave absorption of reduced graphene oxide/$Ni_{0.4}Zn_{0.4}Co_{0.2}Fe_2O_4$ composite at ultrathin thickness. J Electron Mater. 2020; 49: 1721-1727.
180. Ren X, Xu G. Electromagnetic and microwave absorbing properties of NiCoZn-ferrites doped with La^{3+}. J Magn Magn Mater. 2014; 354: 44-48.
181. Zavislyak IV, Popov MA, Solovyova ED, Solopan SA, Belous AG. Dielectric-ferrite film heterostructures for magnetic field controlled resonance microwave components. Mater Sci Eng B. 2015; 197: 36-42.
182. Yue Y, Han P, Dong S, Zhang K, Zhang C, Shang C, et al. Nanostructured transition metal nitride composites as energy storage material. Chin Sci Bull. 2012; 57: 4111-4118.
183. Liao Z, Ma M, Bi Y, Tong Z, Chung KL, Li Z, et al. MoS_2 decorated on one-dimensional $MgFe_2O_4$/MgO/C composites for high-performance microwave absorption. J Colloid Interface Sci. 2022; 606: 709-718.
184. Sun X, Li X, Chen P, Zhu Y. Construction of urchin-like multiple core-shelled Co/CoS_2@NC@MoS_2 composites for effective microwave absorption. J Alloys Compd. 2023; 936: 168243.
185. Wang H, Feng J, Xing H, Lv M, Zong Y, Zhu X, et al. Progress in the use of MoS_2-based composites for microwave absorption. Mater Sci Eng R Rep. 2024; 161: 100838.
186. Wang M, Lin Y, Yang H, Qiu Y, Wang S. A novel plate-like $BaFe_{12}O_{19}$@MoS_2 core-shell structure composite with excellent microwave absorbing properties. J Alloys Compd. 2020; 817: 153265.
187. Rao Y, Long L, Jing T, Qi X, Peng Q, Gong X, et al. Magnetic modulation of core@shell MoS_2-based flower-like multicomponent nanocomposites to improve microwave attenuation. J Colloid Interface Sci. 2022; 608: 2387-2398.
188. Xiong X, Ma H, Mohammed J, Mehrez S, Alamri S, Giang HT, et al. High-performance microwave absorber based on carbon-fibers@TiO_2@$SrFe_{12}O_{19}$@PANI composite. Ceram Int. 2022; 48: 27420-27428.
189. Fan B, Ansar MT, Chen Q, Wei F, Du H, Ouyang B, et al. Microwave-assisted hydrothermal synthesis of 2D/2D $MoS_2/Ti_3C_2T_x$ heterostructure for enhanced microwave absorbing performance. J Alloys Compd. 2022; 923: 166253.
190. Zhang XJ, Wang SW, Wang GS, Li Z, Guo AP, Zhu JQ, et al. Facile synthesis of NiS_2@MoS_2 core-shell nanospheres for effective enhancement in microwave absorption. RSC Adv. 2017; 7: 22454-22460.
191. Sun X, Pu Y, Wu F, He J, Deng G, Song Z, et al. 0D-1D-2D multidimensionally assembled Co_9S_8/CNTs/MoS_2 composites for ultralight and broadband electromagnetic wave absorption. Chem Eng J. 2021; 423: 130132.
192. Tong Z, Liao Z, Liu Y, Ma M, Bi Y, Huang W, et al. Hierarchical Fe_3O_4/Fe@C@MoS_2 core-shell nanofibers for efficient microwave absorption. Carbon. 2021; 179: 646-654.
193. Feng L, Zhao D, Yu J, Zhao Q, Yuan X, Liu Y, et al. Two-dimensional transition metal dichalcogenides based composites for microwave absorption applications: A review. J Phys Energy. 2022; 5: 012001.
194. Negi P, Kumar A. MoS_2 nanoparticle/activated carbon composite as a dual-band material for absorbing microwaves. Nanoscale Adv. 2021; 3: 4196-4206.

195. Zhang W, Zhang X, Zheng Y, Guo C, Yang M, Li Z, et al. Preparation of polyaniline@MoS_2@Fe_3O_4 nanowires with a wide band and small thickness toward enhancement in microwave absorption. ACS Appl Nano Mater. 2018; 1: 5865-5875.
196. Chai J, Cheng J, Zhang D, Xiong Y, Yang X, Ba X, et al. Enhancing electromagnetic wave absorption performance of Co_3O_4 nanoparticles functionalized MoS_2 nanosheets. J Alloys Compd. 2020; 829: 154531.
197. Wang Y, Di X, Fu Y, Wu X, Cao J. Facile synthesis of the three-dimensional flower-like $ZnFe_2O_4$@MoS_2 composite with heterogeneous interfaces as a high-efficiency absorber. J Colloid Interface Sci. 2021; 587: 561-573.
198. Zhang F, Zhang W, Zhu W, Cheng B, Qiu H, Qi S. Core-shell nanostructured CS/MoS_2: A promising material for microwave absorption. Appl Surf Sci. 2019; 463: 182-189.
199. Hassan A, Aslam MA, Bilal M, Khan MS, ur Rehman S, Ma K, et al. Modulating dielectric loss of MoS_2@$Ti_3C_2T_x$ nanoarchitectures for electromagnetic wave absorption with radar cross section reduction performance verified through simulations. Ceram Int. 2021; 47: 20706-20716.
200. Ding X, Huang Y, Li S, Zhang N, Wang J. 3D architecture reduced graphene oxide-MoS_2 composite: Preparation and excellent electromagnetic wave absorption performance. Compos Part A Appl Sci Manuf. 2016; 90: 424-432.
201. Chai J, Zhang D, Cheng J, Jia Y, Ba X, Gao Y, et al. Facile synthesis of highly conductive MoS_2/graphene nanohybrids with hetero-structures as excellent microwave absorbers. RSC Adv. 2018; 8: 36616-36624.
202. Liu J, Jia Z, Zhou W, Liu X, Zhang C, Xu B, et al. Self-assembled MoS_2/magnetic ferrite $CuFe_2O_4$ nanocomposite for high-efficiency microwave absorption. Chem Eng J. 2022; 429: 132253.
203. Giannazzo F, Panasci SE, Schilirò E, Koos A, Pécz B. Integration of graphene and MoS_2 on silicon carbide: Materials science challenges and novel devices. Mater Sci Semicond Process. 2024; 174: 108220.
204. Zhang X, Li Y, Liu R, Rao Y, Rong H, Qin G. High-magnetization FeCo nanochains with ultrathin interfacial gaps for broadband electromagnetic wave absorption at gigahertz. ACS Appl Mater Interfaces. 2016; 8: 3494-3498.
205. Quan B, Liang X, Xu G, Cheng Y, Zhang Y, Liu W, et al. A permittivity regulating strategy to achieve high-performance electromagnetic wave absorbers with compatibility of impedance matching and energy conservation. New J Chem. 2017; 41: 1259-1266.
206. Luo J, Zhang K, Cheng M, Gu M, Sun X. MoS_2 spheres decorated on hollow porous ZnO microspheres with strong wideband microwave absorption. Chem Eng J. 2020; 380: 122625.
207. Zou J, Wang Z, Yan M, Bi H. Enhanced interfacial polarization relaxation effect on microwave absorption properties of submicron-sized hollow Fe_3O_4 hemispheres. J Phys D Appl Phys. 2014; 47: 275001.
208. Yang E, Qi X, Xie R, Bai Z, Jiang Y, Qin S, et al. Core@shell@shell structured carbon-based magnetic ternary nanohybrids: Synthesis and their enhanced microwave absorption properties. Appl Surf Sci. 2018; 441: 780-790.
209. Wang P, Zhang J, Wang G, Duan B, He D, Wang T, et al. Synthesis and characterization of MoS_2/Fe@Fe_3O_4 nanocomposites exhibiting enhanced microwave absorption performance at normal and oblique incidences. J Mater Sci Technol. 2019; 35: 1931-1939.
210. Zhang Y, Gao S, Xing H. Hierarchical core-shell Fe_3O_4@C@MoS_2 composites synergistically enhance microwave absorption. Mater Lett. 2019; 246: 80-83.

211. Wang C, Ma Y, Qin Z, Wang J, Zhong B. Synthesis of hollow spherical MoS_2@Fe_3O_4-GNs ternary composites with enhanced microwave absorption performance. Appl Surf Sci. 2021; 569: 150812.
212. Chen X, Shi T, Wu G, Lu Y. Design of molybdenum disulfide@polypyrrole compsite decorated with Fe_3O_4 and superior electromagnetic wave absorption performance. J Colloid Interface Sci. 2020; 572: 227-235.
213. Liu J, Liang H, Wu H. Hierarchical flower-like Fe_3O_4/MoS_2 composites for selective broadband electromagnetic wave absorption performance. Compos Part A Appl Sci Manuf. 2020; 130: 105760.
214. Wang P, Wang G, Zhang J, Duan B, Zheng L, Zhang S, et al. Excellent microwave absorbing performance of the sandwich structure absorber Fe@B_2O_3/MoS_2/Fe@B_2O_3 in the Ku-band and X-band. Chem Eng J. 2020; 382: 122804.
215. Zhang W, Li L, Zhu W, Yan H, Qi S. Preparation and microwave absorbing performance of MoS_2@Fe_3O_4@PANI composites. J Mater Sci Mater Electron. 2017; 28: 15488-15494.
216. Zhou C, Wu C, Yan M. Hierarchical FeCo@MoS_2 nanoflowers with strong electromagnetic wave absorption and broad bandwidth. ACS Appl Nano Mater. 2018; 1: 5179-5187.
217. Ma M, Zheng Q, Zhu Y, Li L, Cao M. Confinedly implanting Fe_3O_4 nanoclusters on MoS_2 nanosheets to tailor electromagnetic properties for excellent multi-bands microwave absorption. J Materiomics. 2022; 8: 577-585.
218. Li Z, Yang E, Qi X, Xie R, Jing T, Qin S, et al. Outstanding comprehensive performance versus facile synthesis: Constructing core and shell-interchangeable nanocomposites as microwave absorber. J Colloid Interface Sci. 2020; 565: 227-238.
219. Qin Z, Wang C, Ma Y, Sun Z, Zhong B, Li X, et al. MoS_2 nanoflowers decorated with Fe_3O_4/graphite nanosheets for controllable electromagnetic wave absorption. ACS Appl Nano Mater. 2021; 4: 3434-3443.
220. Gai L, Zhao Y, Song G, An Q, Xiao Z, Zhai S, et al. Construction of core-shell PPy@MoS_2 with nanotube-like heterostructures for electromagnetic wave absorption: Assembly and enhanced mechanism. Compos Part A Appl Sci Manuf. 2020; 136: 105965.
221. Xiao J, Qi X, Gong X, Peng Q, Chen Y, Xie R, et al. Tunable and improved microwave absorption of flower-like core@shell MFe_2O_4@MoS_2 (M = Mn, Ni and Zn) nanocomposites by defect and interface engineering. J Mater Sci Technol. 2023; 139: 137-146.
222. Huang W, Tong Z, Bi Y, Ma M, Liao Z, Wu G, et al. Synthesis and microwave absorption properties of coralloid core-shell structure NiS/Ni_3S_4@PPy@MoS_2 nanowires. J Colloid Interface Sci. 2021; 599: 262-270.
223. Liu Y, Ji C, Su X, He X, Xu J, Li Y. Enhanced microwave absorption properties of flaky MoS_2 powders by decorating with Ni particles. J Magn Magn Mater. 2020; 511: 166961.
224. Sun Y, Xu J, Qiao W, Xu X, Zhang W, Zhang K, et al. Constructing two-, zero-, and one-dimensional integrated nanostructures: An effective strategy for high microwave absorption performance. ACS Appl Mater Interfaces. 2016; 8: 31878-31886.
225. Zhang Z, Wang Z, Heng L, Wang S, Chen X, Fu X, et al. Improving the electromagnetic wave absorption properties of the layered MoS_2 by cladding with Ni nanoparticles. J Phys Soc Jpn. 2018; 87: 054402.

226. Ren B, Shen W, Li L, Wu S, Wang W. 3D $CoFe_2O_4$ nanorod/flower-like MoS_2 nanosheet heterojunctions as recyclable visible light-driven photocatalysts for the degradation of organic dyes. Appl Surf Sci. 2018; 447: 711-723.
227. Long L, Yang E, Qi X, Xie R, Bai Z, Qin S, et al. Core@shell structured flower-like $Co_{0.6}Fe_{2.4}O_4$@MoS_2 nanocomposites: A strong absorption and broadband electromagnetic wave absorber. J Mater Chem C. 2019; 7: 8975-8981.
228. Zhu T, Shen W, Wang X, Song YF, Wang W. Paramagnetic CoS_2@MoS_2 core-shell composites coated by reduced graphene oxide as broadband and tunable high-performance microwave absorbers. Chem Eng J. 2019; 378: 122159.
229. Cui X, Liu W, Gu W, Liang X, Ji G. Two-dimensional MoS_2 modified using $CoFe_2O_4$ nanoparticles with enhanced microwave response in the X and Ku band. Inorg Chem Front. 2019; 6: 590-597.
230. Liu H, Zhang M, Ye Y, Yi J, Zhang Y, Liu Q. Porous cobalt ferrite microspheres decorated two-dimensional MoS_2 as an efficient and wideband microwave absorber. J Alloys Compd. 2022; 892: 162126.
231. Bi Y, Ma M, Liu Y, Tong Z, Wang R, Chung KL, et al. Microwave absorption enhancement of 2-dimensional CoZn/C@MoS_2@PPy composites derived from metal-organic framework. J Colloid Interface Sci. 2021; 600: 209-218.
232. Li C, Peng Q, Qi X, Chen Y, Gong X, Wang X, et al. Morphology optimization strategy of flower-like $CoNi_2S_4$/Co_9S_8@MoS_2 core@shell nanocomposites to achieve extraordinary microwave absorption performances. J Colloid Interface Sci. 2022; 606: 1128-1139.
233. Jiang M, Alexpandi R, Lin W, Zhang R, Li S, Zhang Q, et al. Bead-like Co/C@ MoS_2 Composites connected by Multi-Walled carbon nanotubes for high-efficiency electromagnetic wave absorption. Appl Surf Sci. 2024; 660: 159996.
234. Li C, Qi X, Gong X, Peng Q, Chen Y, Xie R, et al. Magnetic-dielectric synergy and interfacial engineering to design yolk-shell structured CoNi@void@C and CoNi@void@C@MoS_2 nanocomposites with tunable and strong wideband microwave absorption. Nano Res. 2022; 15: 6761-6771.
235. Wang Y, Xu J, He P, Liu X, Zuo P, Ma W, et al. Construction of Co/C@MoS_2 core-shell nanocubes with enhanced electromagnetic-wave absorption performance. J Alloys Compd. 2022; 905: 164080.
236. Khan MS, Kim HJ, Taniguchi T, Ebina Y, Sasaki T, Osada M. Layer-by-layer engineering of two-dimensional perovskite nanosheets for tailored microwave dielectrics. Appl Phys Express. 2017; 10: 091501.
237. Quan B, Shi W, Ong SJ, Lu X, Wang PL, Ji G, et al. Defect engineering in two common types of dielectric materials for electromagnetic absorption applications. Adv Funct Mater. 2019; 29: 1901236.
238. Ning MQ, Lu MM, Li JB, Chen Z, Dou YK, Wang CZ, et al. Two-dimensional nanosheets of MoS_2: A promising material with high dielectric properties and microwave absorption performance. Nanoscale. 2015; 7: 15734-15740.
239. Liang X, Zhang X, Liu W, Tang D, Zhang B, Ji G. A simple hydrothermal process to grow MoS_2 nanosheets with excellent dielectric loss and microwave absorption performance. J Mater Chem C. 2016; 4: 6816-6821.
240. Dai J, Yang H, Wen B, Zhou H, Wang L, Lin Y. Flower-like MoS_2@$Bi_2Fe_4O_9$ microspheres with hierarchical structure as electromagnetic wave absorber. Appl Surf Sci. 2019; 479: 1226-1235.

241. Zhang Q, Du Z, Huang X, Zhao Z, Guo T, Zeng G, et al. Tunable microwave absorptivity in reduced graphene oxide functionalized with Fe_3O_4 nanorods. Appl Surf Sci. 2019; 473: 706-714.
242. Xing L, Li X, Wu Z, Yu X, Liu J, Wang L, et al. 3D hierarchical local heterojunction of MoS_2/FeS_2 for enhanced microwave absorption. Chem Eng J. 2020; 379: 122241.
243. Yue Q, Li J, Zhang Y, Cheng X, Chen X, Pan P, et al. Plasmolysis-inspired nanoengineering of functional yolk-shell microspheres with magnetic core and mesoporous silica shell. J Am Chem Soc. 2017; 139: 15486-15493.
244. Liao J, Qiu J, Wang G, Du R, Tsidaeva N, Wang W. 3D core-shell $Fe_3O_4@SiO_2@MoS_2$ composites with enhanced microwave absorption performance. J Colloid Interface Sci. 2021; 604: 537-549.
245. Zhang S, Liu X, Jia C, Sun Z, Jiang H, Jia Z, et al. Integration of multiple heterointerfaces in a hierarchical 0D@2D@1D structure for lightweight, flexible, and hydrophobic multifunctional electromagnetic protective fabrics. Nanomicro Lett. 2023; 15: 204.
246. Lee JS, Kim JW, Lee JH, Son YK, Kim YB, Woo K, et al. Flash-induced high-throughput porous graphene via synergistic photo-effects for electromagnetic interference shielding. Nanomicro Lett. 2023; 15: 191.
247. Liu Z, Tan X, Huang Y, Li W, Yang N, Yuan R, et al. Microwave absorption-based magnetic liquid metal nano-missiles for thermodynamic/immunological cascade hepatoma therapy. Chem Eng J. 2023; 471: 144688.
248. Che R, Wu Z, Quan B, Zhang R, Zhang H, Zhang J, et al. Machine learning-directed fast and high-throughput acquisition of high-efficiency microwave absorbents from infinite design space. Adv Funct Mater. 2023; 33: 2303108.
249. Kung YC, Hosseini N, Dumcenco D, Fantner GE, Kis A. Air and water-stable n-type doping and encapsulation of flexible MoS_2 devices with SU8. Adv Electron Mater. 2019; 5: 1800492.
250. Tsai ML, Su SH, Chang JK, Tsai DS, Chen CH, Wu CI, et al. Monolayer MoS_2 heterojunction solar cells. ACS Nano. 2014; 8: 8317-8322.
251. Quy VH, Vijayakumar E, Ho P, Park JH, Rajesh JA, Kwon J, et al. Electrodeposited MoS_2 as electrocatalytic counter electrode for quantum dot-and dye-sensitized solar cells. Electrochim Acta. 2018; 260: 716-725.
252. Ulaganathan RK, Yadav K, Sankar R, Chou FC, Chen YT. Hybrid InSe nanosheets and MoS_2 quantum dots for high-performance broadband photodetectors and photovoltaic cells. Adv Mater Interfaces. 2019; 6: 1801336.
253. Yu B, Yin L, Wang P, Gong C. Terahertz reconfigurable multi-functional metamaterials based on 3D printed mortise-tenon structures. Virtual Phys Prototyp. 2023; 18: e2230468.
254. Wu F, Hu P, Hu F, Tian Z, Tang J, Zhang P, et al. Multifunctional MXene/C aerogels for enhanced microwave absorption and thermal insulation. Nanomicro Lett. 2023; 15: 194.
255. Chen X, Guo S, Tan S, Ma J, Xu T, Wu Y, et al. An environmentally friendly chitosan-derived VO_2/carbon aerogel for radar infrared compatible stealth. Carbon. 2023; 213: 118313.
256. Xiang X, Yang Z, Fang G, Tang Y, Li Y, Zhang Y, et al. Tailoring tactics for optimizing microwave absorbing behaviors in ferrite materials. Mater Today Phys. 2023; 36: 101184.
257. Khalid MY, Umer R. Towards a new era of 2D materials-based multifunctional composites film: From innovation to evolution. Adv Ind Eng Polym Res. 2024. doi: 10.1016/j.aiepr.2024.04.002.
258. Rehman SU, Xu S, Li Z, Tao T, Zhang J, Xia H, et al. Hierarchical-bioinspired MOFs enhanced electromagnetic wave absorption. Small. 2024; 20: 2306466.

259. Liu M, Zhao B, Pei K, Qian Y, Yang C, Liu Y, et al. An ion-engineering strategy to design hollow FeCo/$CoFe_2O_4$ microspheres for high-performance microwave absorption. Small. 2023; 19: 2300363.
260. Jin H, Zhou J, Tao J, Gu Y, Yu C, Chen P, et al. Commonly neglected ester groups enhanced microwave absorption. Small. 2023; 19: 2304536.
261. Yan J, Zheng Q, Wang SP, Tian YZ, Gong WQ, Gao F, et al. Multifunctional organic-inorganic hybrid perovskite microcrystalline engineering and electromagnetic response switching multi-band devices. Adv Mater. 2023; 35: 2300015.
262. Shu JC, Cao MS, Zhang YL, Cao WQ. Heterodimensional structure switching multispectral stealth and multimedia interaction devices. Adv Sci. 2023; 10: 2302361.
263. Wang XX, Zheng Q, Zheng YJ, Cao MS. Green EMI shielding: Dielectric/magnetic "genes" and design philosophy. Carbon. 2023; 206: 124-141.
264. Wang YC, Wang YZ, Shu JC, Cao WQ, Li CS, Cao MS. Graphene implanted shape memory polymers with dielectric gene dominated highly efficient microwave drive. Adv Funct Mater. 2023; 33: 2303560.
265. Luo J, Yang X, Xue Y, Yang C, Yang Z, Cai Z, et al. High-performance, multifunctional, and designable carbon fiber felt skeleton epoxy resin composites EP/CF-$(CNT/AgBNs)_x$ for thermal conductivity and electromagnetic interference shielding. Small. 2024; 20: 2306828.
266. Liu Y, He X, Wang Y, Cheng Z, Yao Z, Zhou J, et al. Controlled synthesis of MOF-derived nano-microstructure toward lightweight and wideband microwave absorption. Small. 2023; 19: 2302633.
267. Jiang H, Wang C, Cui B, Xu X, Li M, Xu Z, et al. Lotus leaf derived NiS/carbon nanofibers/porous carbon heterogeneous structures for strong and broadband microwave absorption. Small. 2023; 19: 2304918.
268. Shu JC, Wang YZ, Cao MS. PEDOT: PSS-patched magnetic graphene films with tunable dielectric genes for electromagnetic interference shielding and infrared stealth. J Mater Sci Technol. 2024; 186: 28-36.